BIO-INSPIRED MATERIALS FOR ENERGY STORAGE APPLICATIONS

A Thesis

by

SIDDHI GAJANAN MEHTA

Submitted to the Office of Graduate and Professional Studies of
Texas A&M University
in partial fulfillment of the requirements for the degree of

MASTER OF SCIENCE

Chair of Committee,	Hong Liang
Committee Members,	Efstratios N. Pistikopoulos
	Mahmoud El-Halwagi
Head of Department,	Efstratios N. Pistikopoulos

December 2019

Major Subject: Energy

ABSTRACT

Due to the immense demand for flexible supercapacitors, increasing amount of research is being done to develop low-cost and smart solutions. To date, electrodes made of eco-friendly materials have been either expensive or of limited use. This research investigates design, synthesis, and electrochemical evaluation of a novel class materials as electrodes. A group of solid-state, lightweight, low cost, and plant-based electrodes for supercapacitors are studied using experimental approaches. The biomaterial lignin is studied extensively for its use as an active material in those electrodes. For this purpose, the transition metal oxide MnO_2 and $NiWO_4$ nanoparticles are introduced to the lignin matrix, separately. To avoid the risks of using aqueous electrolytes, an organic gel polymer electrolyte PVA/H_3PO_4 is used. They show high specific capacitance values, with ~90% energy retention. The electrochemical performance exhibited by these lignin-based electrodes match the state-of-the-art results, and is superior in some cases. Due to the simplicity of the design process, these electrodes are a cost-effective option to the expensive eco-friendly materials currently in use. The remarkable electrochemical performance of these electrodes makes them useful for a wide variety of electronics. This new approach to fabricate electrodes from green sources, with simple processing and cost-effectiveness, marks an important step towards green energy technology development.

This thesis includes 6 chapters. Following the first chapter of introduction and literature review, a hypothesis and a problem statement is discussed in the second chapter. The

third chapter talks about the interaction of combining lignin with a transition metal oxide and the fourth chapter is a study on the effects of adding a biomaterial to this combination. In the fifth chapter, novel nanoparticles are introduced into the lignin matrix and their capacitive performance is studied. The final chapter analyzes the results obtained in this research and provides conclusions and recommended future studies.

DEDICATION

This thesis is dedicated to the memory of my grandmother Sangeeta Butala. Although she was my inspiration to pursue research, she was unable to see my graduation. This is for her.

Thank you to my adviser, Dr. Liang who patiently guided me in this process and my mentor Swarn Jha who kept me on track.

I dedicate this thesis to my mother, who always told me the sky is the limit for all my dreams, to my father who taught me that no obstacle is too big to overcome, to my grandfather, without whom I wouldn't have reached here and to my best friend Ayesha who never let me give up.

This thesis is dedicated to my sister who always supported, encouraged and reminded me to have faith in myself and my abilities to pursue my dreams.

ACKNOWLEDGEMENTS

I would like to thank my committee chair, Dr. Liang, and my committee members, Dr. Pistikopoulos, and Dr. El-Halwagi, and my mentor Swarn Jha for their guidance and support throughout the course of this research.

Thanks also go to my friends and colleagues and the department faculty and staff for making my time at Texas A&M University a great experience.

Finally, thanks to my family for their encouragement, patience and love.

CONTRIBUTORS AND FUNDING SOURCES

Contributors

This work was supervised by a thesis committee consisting of Dr. Hong Liang of the Department of Mechanical Engineering and the Department of Material Sciences, Dr. Efstratios N. Pistikopoulos of the Department of Chemical Engineering and Texas A&M Energy Institute, and Dr. Mahmoud El-Halwagi of the Department of Chemical Engineering.

The novel nanoparticles used in Chapter 5 were synthesized and provided by Dr. Subrata Kundu of CSIR-Central Electrochemical Research Institute (CECRI), Karaikudi - 630 003, INDIA

All the other work conducted for the thesis was completed by the student independently.

Funding Sources

Graduate study was supported by a fellowship from Texas A&M Energy Institute.

TABLE OF CONTENTS

Page

LIST OF FIGURES

Page

1. INTRODUCTION

The purpose of this chapter is to provide readers with the background needed in order to understand the undertaken research. This chapter discusses about lignocellulose, an emerging class of materials, and its application in energy storage systems. Here, we discuss the molecular structure of its various components, and the methods of pretreatment and extraction currently in use.

1.1. Literature Review

Since the late 1980s, increasing population and consumption have been the driven force in energy demands and prices. To meet this demand, the amount of fuel being burnt and the cost of fuel have increased immensely. The energy that we produce, a certain amount of it is wasted due to the lack of proper storage technologies. The current energy storage technologies are either too expensive or harmful to the environment. This has enabled research efforts on renewable sources, with a major requirement of efficient and cost-effective storage systems[1].

An efficient energy storage system (ESS) is an essential requirement for any electrical energy being generated from renewable resources. Batteries as well as electrochemical capacitors (supercapacitors) are the main ESS currently in use but, they come with their own respective flaws. On the positive side, electrochemical capacitors have high power densities, and fast charge-discharge capability, store 10-100 times more energy than batteries, and have a long cycling life (> 100,000). However, electrochemical capacitors

have lower energy densities (1 Wh kg^{-1} – 30 Wh kg^{-1}), almost 10 – 50 times lesser than Li-ion batteries[2]. This means only part of the energy stored is accessible for use. This is due to the internal resistance of the capacitor and the voltage drop in the system. The materials used, process followed, and the synthesis method, dictates the electrochemical performance of a supercapacitor. The materials used, the process followed, the synthesis method, and the design and assembly dictate the electrochemical performance of a supercapacitor. Widely used materials include conducting polymers, transition metal oxides, and carbon. The most commonly used carbon materials are activated carbon, carbon black, carbon nanotubes, and graphite.

In the last decade, the development of green carbon materials or biomaterials, produced from agro-industrial waste, has attracted special attention. The main advantages of those biomaterials are their abundance, low cost, and waste mitigation[3]. The chemical polarity, high surface area, and pore structure mostly depend on the pretreatment process and precursor material[4]. Various precursor materials derived from agricultural waste, are used to prepare porous carbons for electrochemical applications. In this study, we discuss these bio-derived materials and the vast research done on them. These materials have been used as binders, electrodes, and electrolytes for energy storage devices. To make these devices more efficient, their extraction process, the structure, as well as their design, construction, and synthesis has been studied extensively.

1.2. Storage mechanisms in electrochemical devices

1.2.1. Supercapacitors

Supercapacitors (SC) store energy using either ion surface assimilation (electrical double-layer) or pseudocapacitance (redox reactions on the surface). The charge-discharge mechanism of SCs is predominantly due to the charged double-layer. It enables the reversible electrostatic accumulation of ions on the electrode surface. One electrode works as a cathode and one as an anode. When polarized, the cathode releases positive ions and the anode releases negative ions. Diffusion of these ions through the electrolyte occurs and forms a condensed layer parallel to the electrode surface. The total capacitance of a SC is:

$$1/C = 1/C_C + 1/C_A \quad (1)$$

where, C = total capacitance; C_C = capacitance of the cathode; C_A = capacitance of the anode.

Supercapacitors store almost 3-30 times less charge than batteries [33]. They offer higher power at the same volume, have excellent charge-discharge reversibility (~90–95%), and long cycling life (up to 500,000) [34]. This makes them an excellent choice for applications that require power bursts. To avoid the energy and power density characteristics exhibited by supercapacitors, they can be coupled with batteries to form a hybridized battery-based energy storage system. Few applications of ECs currently in use include electric vehicles, electric tools, devices for digital communication, cellphones, digital cameras, and to store the energy generated by photovoltaic cells [35, 36].

The materials mainly used for SCs include transition metal oxides, different types of carbon materials, and conductive polymers to enhance the electrochemical conductivity [37]. As mentioned above, these materials are cost-effective and can be manufactured into ECs simply, compared to other materials [38]. The main problem with SCs is long-term stability during cycling. Degradation of the SC may occur during cycling, due to the swelling and shrinking of the electroactive materials. The lack of a complete understanding of the charge-storage mechanisms in polymer electrodes is another issue that needs to be overcome [39].

1.2.2. Batteries

Fundamentally, a battery converts stored chemical energy into electrical energy. Similar to a supercapacitor (SC), it contains a cathode and an anode. Through an electrolyte, ions are transferred between the electrodes, thus allowing the current to flow out of the battery. Advances in technology and materials have greatly helped to increase the output of battery systems, at an economic cost [35]. The 3 major types of solid-state batteries currently in use are, Lithium-ion, Nickel-Cadmium, and Sodium-Sulfur batteries.

1.3. Lignocellulose Biomass

Any substance extracted from industrial and agricultural waste is called biomass. Biomass materials are plant-based, with 3 major components, i.e. hemicellulose, cellulose and lignin, as illustrated in Figure 1.1. These components are called lignocellulosic biomass. They are fused by covalent linkages or non-covalent forces and are strongly intermeshed.

In this review, current research focused on waste materials for electrochemical capacitor applications is discussed. The lignocellulosic biomass has unique structural and chemical diversity that varies with the originating species. Their availability, low price, biocompatibility, and the fact that they are renewable gives them their biggest advantage. Biomass not only shows a great potential for use in energy storage systems but also in removal of contaminants[5-7].

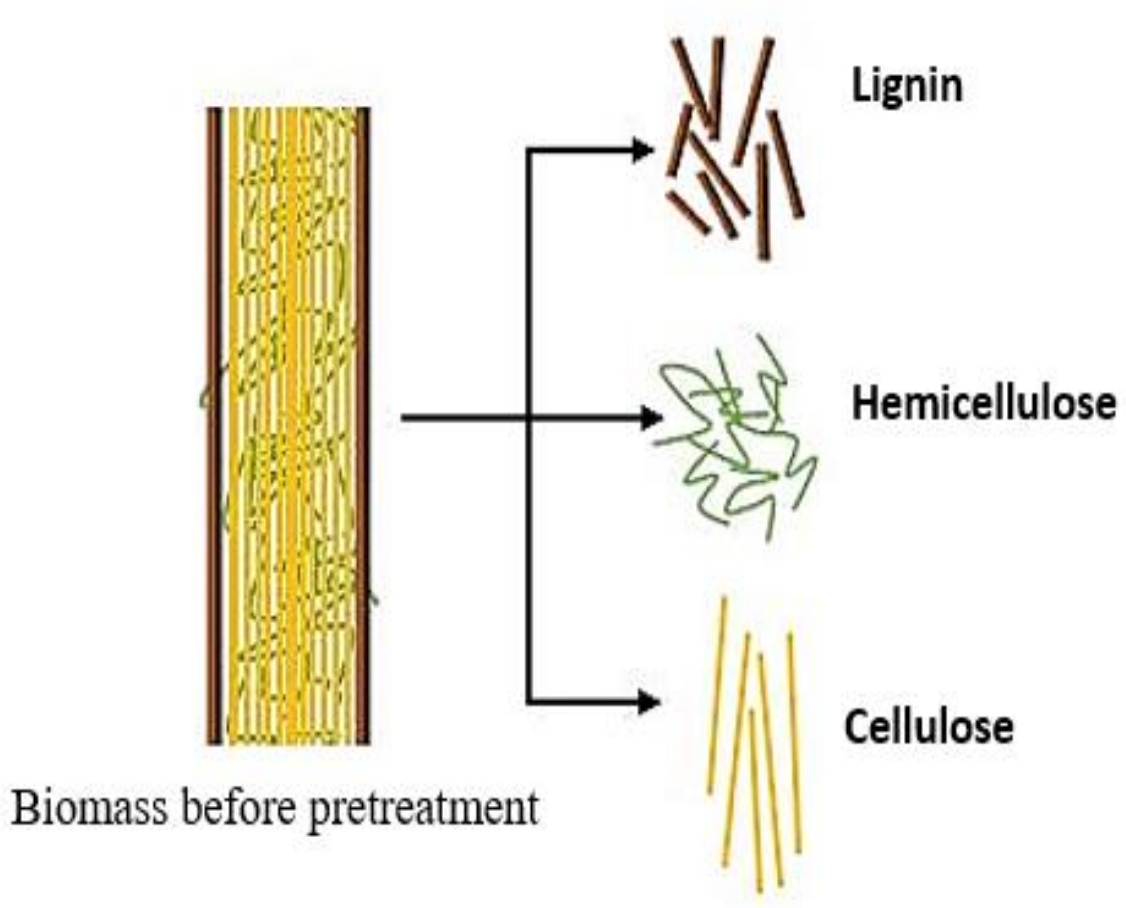

Figure 1.1: Separated components of lignocellulosic biomass after pretreatment

Due to their intricate structures, carbon electrodes have the ability to boost the energy density in supercapacitors. There is a spike in energy density which can be attributed to the increment in capacitance of both positive and negative electrodes [40]. There are many studies that focus on replacing the carbon electrode with redox-active or pseudocapacitive materials as they exhibit higher capacitance. However, despite the increase in capacitance of the cell, they still have low power density and cycle life. These drawbacks can be overcome by using carbonaceous materials, derived from plants, as a matrix for the electrode and decorating them with different functionalities.

1.3.1. Cellulose

One of the most abundantly available organic polymers, cellulose is present in the wall of the plant cells. It is made up of D-Glucose units (pyranose), a six-carbon ring (Refer Figure 1.2). Each pyranose ring consists of 3 hydroxyl groups, causing the interaction between one another. This interaction leads to the formation of the intra- and inter-molecular hydrogen bonds. These bonds give cellulose its unique mechanical strength, chemical stability and crystalline structure. Cellulose is also called a polysaccharide of anhydro-gluco-pyranose. This is because the pyranose rings, linked to each other by acetal bonds cause the loss of a molecule of water[8, 9].

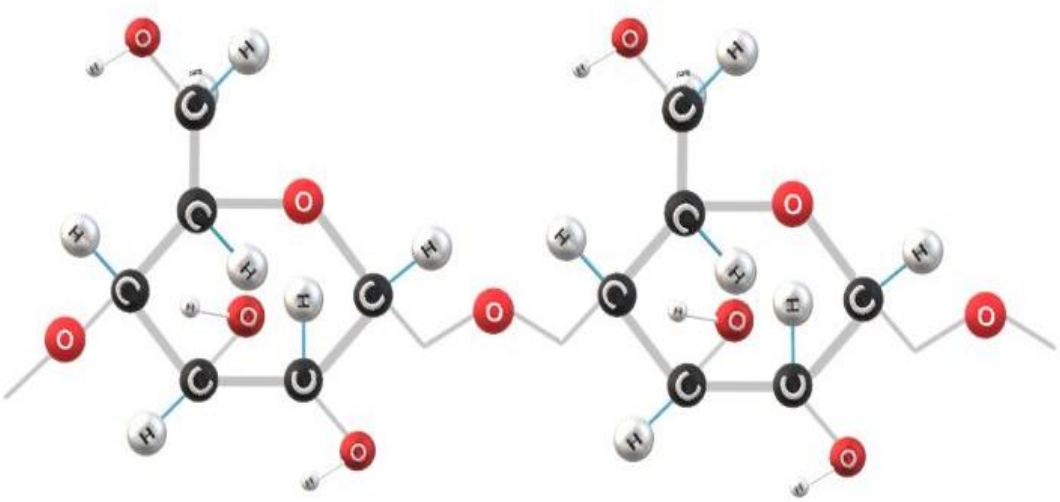

Figure 1.2: Model of the cellulose molecule

1.3.2. Hemicellulose

The polymer that encloses the cellulose fibers and thereby acts as a connecting link between cellulose and lignin, is called hemicellulose. The structural elements contain various different monomers, like glucose, galactose, mannose, xylose, arabinose, and glucuronic acid (Figure 1.3)[10]. The 3-methoxy galacturonic acid is linked with xylose units, thus forming short-chain compounds. Compared to the crystalline, hydrolysis-resistant structure of cellulose, hemicellulose has a little physical strength and is amorphous in nature. It can be easily hydrolyzed by dilute bases, and acids, hemicellulose enzymes.

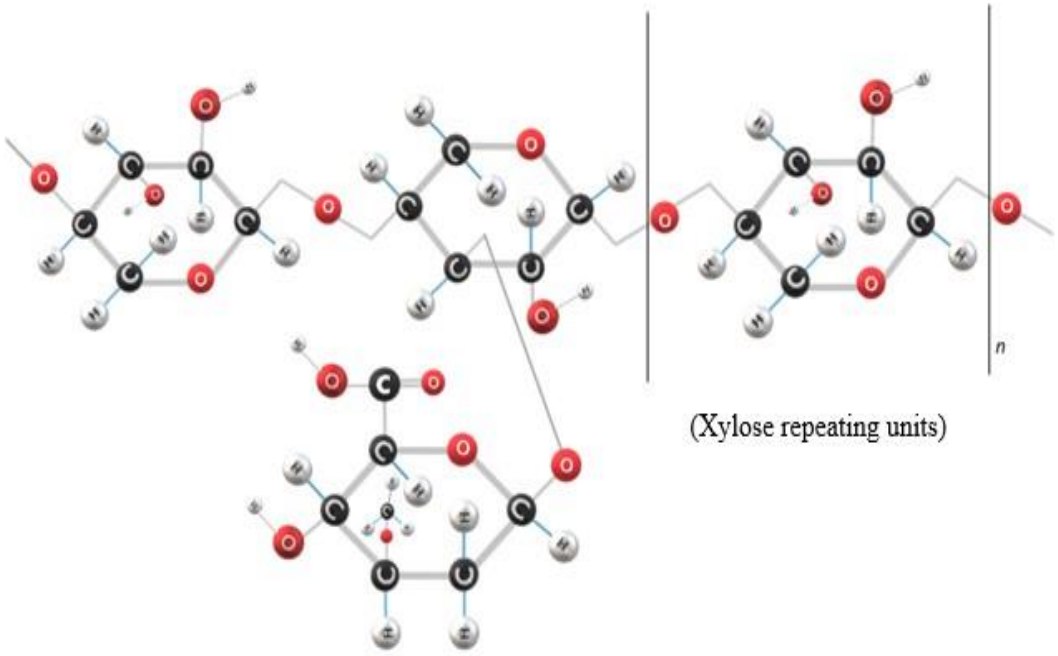

Figure 1.3: Model of the hemicellulose molecule

1.3.3. Lignin

The structure of a lignin molecule contains an assortment of hydroxyl- and methoxy-groups which are bonded differently. The three main monomeric units of lignin are coniferyl, p-coumaryl, and sinapyl alcohol groups (Refer Figure 1.4)[11]. Lignin can be found mainly in fiber's outer layers. It is responsible for the structural rigidity of the fibers and holds the polysaccharides together. Lignin constitutes for approximately 33% in softwoods and 25% in hardwoods. Lignin acts a binder between the hemicellulose and cellulose. Its structure varies based on the source of biomass and the extraction method used.

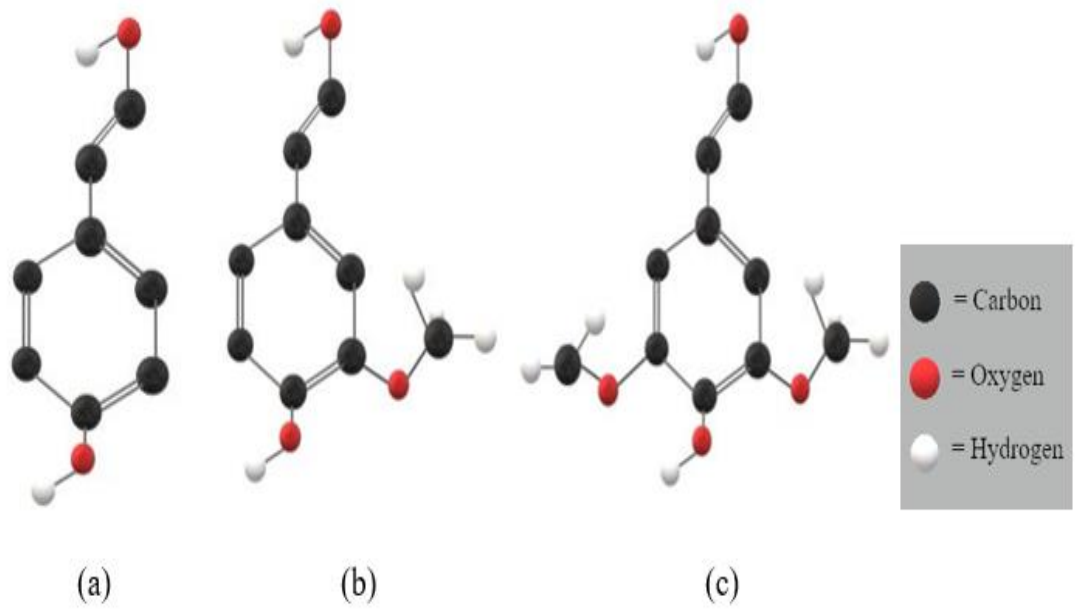

Figure 1.4: Monomeric units of lignin macromolecules: (a) p-coumaryl alcohol, (b) coniferyl alcohol, and (c) sinapyl alcohol

1.4. Extraction & Processing of Lignocellulosic Biomass

As mentioned earlier, lignocellulosic biomass consists of three major materials, namely, cellulose, hemicellulose, and lignin. These materials require pretreatment to convert them from them their native form to a form where enzymatic hydrolysis can be effective. The method of pretreatment used depends upon the source of the biomass. They can be further converted depending upon the application by using thermochemical methods, carbonization (slow pyrolysis), and fermentation. Pretreatment of biomass can be classified in 4 categories, namely; physical, chemical, physiochemical, and biological.

1.4.1. Physical (Mechanical) Pretreatment

1.4.1.1. Physical Comminution (Particle/Fragment Reduction)

Physical pretreatment is mainly used for particle reduction to the desired size and reducing the crystallinity of the lignocellulosic biomass. This is done for easing material handling, increasing the specific surface area and surface/volume ratio, and to reduce the degree of polymerization. This usually involves different milling processes like, two-roll milling, hammer milling, colloid milling, etc. or chipping or grinding[12]. The economic feasibility, high energy consumption, and equipment depreciation, are important factors that need to be considered for this pretreatment process.

1.4.1.2. Extrusion

Extrusion is an operation to create objects a fixed, cross-section. This is done by forcing the biomass through a die of required cross-section. In extrusion process, biomass is treated at temperatures > 300°C. In doing so, the material expands on exiting the die. It is used mainly to produce residual char & gaseous products[13]. The lignocellulosic structure is disrupted by the screw speed and barrel temperature. This in turn causes defibrillation, fibrillation and shortening of lignocellulosic fibers, thus increasing the arability of carbohydrates for enzymatic attack.

1.4.2. Chemical Pretreatment:

1.4.2.1. Liquid Hot Water

This is a hydrothermal treatment that doesn't require any rapid decompression or additives. The most commonly used temperature is 170°C - 230°C, with pressure > 5MPa[14]. The high pressure is used to ensure the liquid state of water under high temperatures. This makes cellulose more easily accessible by removing hemicellulose from the biomass. The slurry obtained after the pretreatment is filtered to obtain solid cellulose-enriched fraction and a hemicellulose-rich liquid fraction. Due to better pH control, the degradation of polysaccharides is reduced. This process shows potential for high recovery of hemicellulosic sugars in oligomeric form, thus reducing undesired degradation and high yield of enzymatic hydrolysis of various pretreated biomass. Approximately, 40%-60% of the biomass is dissolved (cellulose: 4-22%; lignin: 35-60%; hemicellulose – 100%). The variances in the results is due to the recovery of hemicellulose being obstructed by the high lignin solubilization [15].

1.4.2.2. Acid Hydrolysis

Pretreatment using acids causes solubilization of lignin and hemicellulose, making cellulose accessible to enzymes. There are 2 types of acid hydrolysis; weak acid hydrolysis which uses diluted acid pretreatment and strong acid hydrolysis which uses concentrated acids for pretreatments.

1.4.2.2.1. Weak Acid Hydrolysis

Being one of the most effective and feasible pretreatment methods, it can be performed in 2 ways.

1) High temperature (>160°C), less time, with continuous flow process (low-solid loading)

2) Low temperature (≤ 120°C), more time (~30-90 mins), with batch process (high-solids loading)

Dilute acid, generally H_2SO_4, is sprayed on the raw biomass which is heated and held at 160°C - 220°C, for a few minutes. This is leads to the hydrolysis of hemicellulose, release of monomeric sugars, and oligomers. The removal of hemicellulose leads to increased porosity and improved enzymatic digestibility[16]. Organic acids have also been used for weak acid hydrolysis.

1.4.2.2.2. Strong Acid Hydrolysis

This method uses concentrated acids such as, HCL, H_2SO_4, H_3PO_4, HNO_3, glycolic acid, oxalic acid, formic acid, etc. They are very useful for cellulose hydrolysis nullifying the further need of enzymes[12]. By using H_2SO_4 and HCL the process could be inexpensive, but the high temperatures, and high energy input requirement, makes it costly. Due to the corrosive nature of the acids at high temperatures, the process requires reaction vessels that are specifically resistant to these conditions.

1.4.2.3. Alkaline Hydrolysis

In alkaline hydrolysis, alkali such as. NaOH, KOH, $Ca(OH)_2$, and NH_4OH are used to treat the biomass at normal pressure and temperature. This process enables efficient removal of lignin, as well as the acetyl and uronic acids in hemicellulose[17]. This enhances the enzyme's accessibility that degrades hemicellulose. This process also improves cellulose digestibility, and effectiveness of lignin solubilization. As compared to acid hydrolysis, hemicellulose and cellulose solubilization is minor[18]. NaOH is the most effective for increase in the internal surface are of cellulose, disruption of lignin structure, and reducing the degree of crystallinity and polymerization[19-21]. Another widely used alkali is lime ($Ca(OH)_2$), as it not only removes the acetyl groups and lignin-carbohydrate ester, but also causes enhancement of cellulose digestibility. Adding oxygen to the NaOH/ $Ca(OH)_2$ treatment increases lignin removal, thus increasing the efficiency of the pretreatment. This pretreatment has been proven successful for various lignocellulosic biomass[22, 23].

1.4.2.4. Ozonolysis

Ozone (O_3) is a very powerful oxidizing agent, which on treatment with biomass causes lignin degradation, but does not affect cellulose or hemicellulose. In this treatment method, O_3 gas is passed through a reaction vessel that contains the biomass. The vessel could have any different kinds of arrangements[24, 25]. It attacks the aromatic rings present in lignin, and thus can be used for disruption of the structure of various lignocellulosic biomass[12, 24]. Usually performed at room temperature and pressure, Ozonolysis doesn't produce any toxic residues.

1.4.2.5. Organosolv Pretreatment

In organosolv pretreatment, the biomass is treated with aqueous or non-aqueous organic solvents to extract lignin before cellulose fraction's enzymatic hydrolysis. The most common solvents used include, ethanol, methanol, acetone, and ethylene glycol[26]. The temperature used depends upon the catalyst used and the type of biomass[27]. The catalysts generally used are organic or inorganic acids[12]. The solvent has to be removed before fermentation can occur as it can be an inhibitor for fermentation and enzymatic hydrolysis. Some of the organic solvents can be used as catalysts as well at high temperatures. The glycerol-based organosolv pretreatment resulted not only 98% cellulose retention, but also removal of 65% lignin and 70% hemicellulose[28]. This process is highly used for lignin extraction, because of the high quality of lignin produced. Though the process is extremely efficient, it is very expensive due to the safety measures required and the removal of these solvents[29].

1.4.3. Physiochemical Pretreatment

1.4.3.1. Steam Explosion

In steam explosion pretreatment, biomass is chipped and treated with high pressure for a certain time (30 s – 20 min), after which the pressure is suddenly decreased. This is known as explosive decompression. It is of the most common pretreatment methods used for lignocellulosic biomass [30,31]. During this pretreatment, the autohydrolysis of the acetyl groups occurs. Autohydrolysis commences at high temperatures, forming acetic acid from the aforementioned acetyl groups [32,33]. The separation of fibers occurs due to explosive

decompression. This results in degraded transformation of hemicellulose and lignin, thereby increasing the cellulose hydrolysis potential [32]. The parameters that influence this process are (1) applied temperatures, (2) content of moisture present, (3) residence time, (4) size of the particles.

Advantages of Steam Explosions include; improved enzymatic hydrolysis, lower capital cost, lesser environmental impact, higher energy efficiency, high sugar recovery, no acid catalysts required except for softwoods, economically feasible at industrial level [34]. The main drawbacks of this process are the toxic components formation and partial degradation of hemicellulose [35]. To obtain the final chip size before being pretreated makes up to 1/3rd of power consumption. A separate detoxification step is required to remove the unnecessary byproducts, which increases the overall cost[36, 37].

1.4.3.2. AFEX

In Ammonia fiber/free explosion or AFEX, liquid ammonia is used to treat the biomass for a certain temperature (90-100˚C) which then undergoes a rapid pressure release. This causes the liquid ammonia to expand, which in turn causes the disruption of biomass fibers and cellulose undergoes partial decrystallization. This process used to modify the faction of lignin and crystallinity of cellulose in the lignocellulosic biomass. This process doesn't produce any inhibitors, thus reducing the water wash cost. Under optimal conditions, ~ 90% of hemicellulose and cellulose is converted. AFEX shows higher effectiveness on the biomass containing lesser amounts of lignins. A problem with this process is ammonia recovery, which is very expensive.

1.4.3.3. CO2 Explosion

CO_2 is used as supercritical fluid, for the effective removal of lignin, due to the supercritical pretreatment conditions[38]. The addition of solvents like ethanol, improves the delignification at high pressures. CO_2 molecules have the ability to penetrate small pores that are approachable to water and ammonia molecules, thus making it comparable in size. Cellulose and hemicellulose disruption occur, thus increasing the surface area available for enzymatic attacks. Due to the low cost availability, easy recovery, non-toxic and non-flammable nature of CO_2, and lower inhibitor formation, makes it a more economically feasible option as compared to steam and ammonia pretreatment[39, 40].

1.4.4. Pyrolysis of Lignocellulosic Materials

There are three types of pyrolysis processes based on the required operating conditions: flash pyrolysis, fast pyrolysis, slow pyrolysis (carbonization).

Slow pyrolysis occurs under a slow heating rate (400˚C - 600 ˚C). Due to this, there is a significant production of solid, liquid and gas products of the biomass. During slow pyrolysis, water elimination, the formation of different organic groups, bond breakage, etc. takes place [41, 42]. Fast pyrolysis (400˚C - 700 ˚C) is generally used when the production is focused mainly on liquid and/or gaseous products [41]. Vacuum pyrolysis produces products rapidly at slow heating rates [43]. Flash pyrolysis (> 600 ˚C) occurs when the heating rates are high and the temperatures are moderate and produces lesser gas and tar, in comparison to slow pyrolysis [44]. For maximum yield of products, the

temperature has to be low, and heating rate has to be high. Low temperature and low rate of heating are ideal for high char production [45, 46].

1.5. Calculations for the Capacitive Performance of Lignocellulosic Materials

The maximum specific capacitance of an electrode is used to evaluate the performance of the electrochemical energy system (ESS). Three elements of ESS were selected to be investigated, specific capacitance, energy density, and power density.

The calculations for the above the above-mentioned parameters of capacitive performance are as follows:

1) Specific Capacitance:

$$C = \Delta Q / (m \times \Delta V) \quad \text{(3 electrode system)} \quad (2)$$

$$C = (2 \times \Delta Q) / (m \times \Delta V) \quad \text{(2 electrode system)} \quad (3)$$

Where, C = specific capacitance; ΔQ = difference in charge during charge and discharge cycles respectively; ΔV = difference in potential.

2) Energy Density:

$$E = (C \times \Delta V^2) / (2 \times 3.6) \quad (4)$$

Where, E = energy density; C = specific capacitance; ΔV = difference in potential

3) Power Density:

$$P = (3.6 \times E) / \Delta t \quad (5)$$

Where, P = power density; E = energy density; Δt = discharge time

1.6. Summary

This chapter has summarized the source, extraction, processing, pre-treatment, and use of lignocellulosic biomass for application as electrode materials. The challenges faced by the lignocellulose-derived electrodes is unstable capacitive performance of these electrochemical capacitors. The reasons for this instability are pore structure and distribution, different physiochemical properties due to different sources of biomass, surface functionalities, conductivity, and wettability. Apart from these parameters, the surface chemistry, extraction and pretreatment methods, electrode preparation method, electrolyte system used and the testing method and equipment as play a major role in capacitive performances of lignocellulose-derived electrodes. This research will investigate novel electrodes for batteries and supercapacitors.

2. MOTIVATIONS & OBJECTIVES

Chapter 1 discussed about the different components of the lignocellulosic biomass along with their molecular structure, extraction and pretreatment methods. The electrochemical conductivity and capacitive performance of these materials has been studied for more than a decade. The main advantages of those biomaterials are their abundance, low cost, waste mitigation and their environmentally friendliness [3]. Various precursor materials derived from agricultural waste, are used to prepare porous carbons for electrochemical applications. These materials have been used as binders, electrodes, and electrolytes for energy storage devices, mainly in supercapacitors.

2.1. Problem Statement

Though a supercapacitor has high capacitance and power density, it has very low energy density compared to batteries. Additionally, they have liquid electrolytes which pose a risk on their own. The materials generally used for supercapacitors are synthetic polymers. In this research, experiments are proposed to synthesize electrode material using environmentally friendly, plant-based materials. The risk posed by liquid electrolytes is sought to be eliminated with the use of a gel electrolyte.

2.2. Hypothesis

Lignocellulose-based electrodes in combination with organic gel polymer electrolytes could be a cost-effective and environmentally friendly option for energy storage systems.

2.3. Objectives of this Research

The main objective of this research is to study the electrochemical properties of the plant-based electrodes used in supercapacitors. The biomaterial selected for this purpose is lignin. The changes the supercapacitor undergoes, the stability of a lignin-based system, and the comparison of the behaviors exhibited by lignin when combined with various other materials, will be studied. This research will study the:

1) effects of transition metals on lignin
2) effects of transition metal on lignin combined with another biomaterial (Activated Carbon)
3) effects of novel nanoparticles ($NiWO_4$) on lignin

The proposed research is conducted primarily through experimental approaches. The overall approach is illustrated in Figure 2.1. Firstly, a comprehensive review and selection was conducted through literature review. We identified a key material, lignin, for this research. Two areas of research were carried out. The capacitive behavior of lignin decorated with MnO_2 was studied as a reference. Then newly synthesized nanoparticles of $NiWO_4$ were introduced into the lignin matrix. The electrolyte proposed is an organic gel polymer electrolyte, PVA/H_3PO_4. A paper separator will be coated with a film of the gel electrolyte and sandwiched between the 2 electrodes to form a solid-state asymmetrical supercapacitor. The capacitive performance exhibited in both cases is studied extensively to synthesize novel plant-based electrodes for batteries and supercapacitors.

Image Analysis Study via Scanning Electron Microscope (SEM) will be used to study the adhesion between the substrate and the active material, as well as the interface between

the electrode and the electrolyte. The electrochemical performance is done using Gamry Instruments & Potentiostat. To study the capacitive performance the supercapacitor will be studied using three electrochemical tests; Cyclic Voltammetry (CV), Cyclic Charge-Discharge (CCD) and Electrochemical Impedance Spectroscopy (EIS).

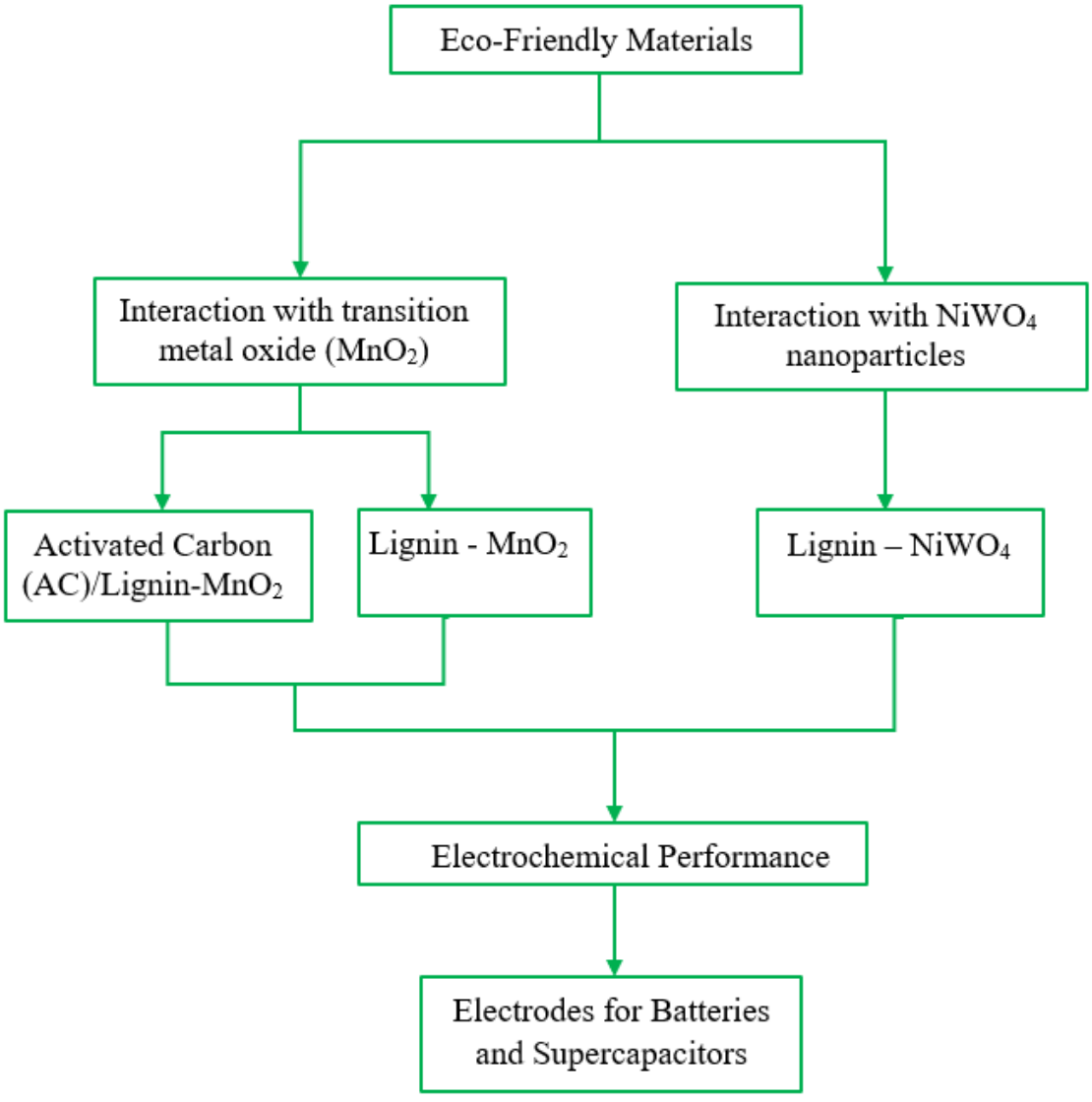

Figure 2.1: Overall research approach

The following 6 chapters report the experimental results and findings in above mentioned three areas. Chapter 3 and 4 discuss the effects of the MnO_2 particles. Chapter 5 studies the interaction of lignin and the novel $NiWO_4$ particles, with Chapter 6 summarizing the conclusions of this study and providing future recommendations.

3. MNO_2 DECORATED, LIGNIN BASED NOVEL ELECTRODES

This chapter discusses about the capacitive performance of the electrode made from the biomaterial lignin, derived from industrial waste. Here, lignin has been decorated with a transitional metal oxide (MnO_2) particles to improve the performance of the electrode. The impact of MnO_2 particles on lignin has been studied using three electrochemical tests; Cyclic Voltammetry (CV), Cyclic Charge-Discharge (CCD) and Electrochemical Impedance Spectroscopy (EIS).

3.1. Preparation of Lignin/MnO_2 Composite Electrode

First, a 50 ml $KMnO_4$ solution of 47.5µmol was made. Then 0.3 g of alkaline lignin powder (TCI) was taken in an autoclave with a Teflon liner, and 50 ml of $KMnO_4$ solution, prepared earlier, was added to it. Hydrothermal treatment was carried out at 160^0 C for 1 hour. The resultant solution was allowed to cool down at room temperature. The excess liquid was drained, and the slurry was dried in a vacuum oven overnight at 50^0C. The powder obtained was mixed with PVDF in the ratio 4:1, and 2 ml of NMP was added to the slurry. The slurry was coated on an aluminum foil substrate cut in the form of a circular plate of diameter 4 cm. The adjoining strips of the foil were 1 cm wide and 3 cm long. The coated foil was heated in a vacuum oven for 4 hours at 100°C to obtain the Lignin/MnO_2 composite electrode.

3.2. Preparation of PVA/H_3PO_4 Gel Electrolyte

A non-aqueous gel made up of PVA/H_3PO_4 was prepared. To make this gel, 1g of PVA was added to 10 ml water. The resultant mixture was stirred over a magnetic heater at 80°C for 40 mins and 0.8g H_3PO_4 was added to the resultant solution. The solution was stirred for another 20 mins at 70°C. A commercial paper, was dipped in it and used as a separator for the supercapacitor.

3.3. Fabrication of Solid-state Asymmetric Supercapacitor

To fabricate the supercapacitor, the electrodes made earlier were used. The Al/lignin-MnO_2 composite electrode was used as the positive electrode and Al/AC was used as the negative electrode. The two electrodes were sandwiched with the gel electrolyte in between. The schematic of the methodology is shown in Figure 3.1.

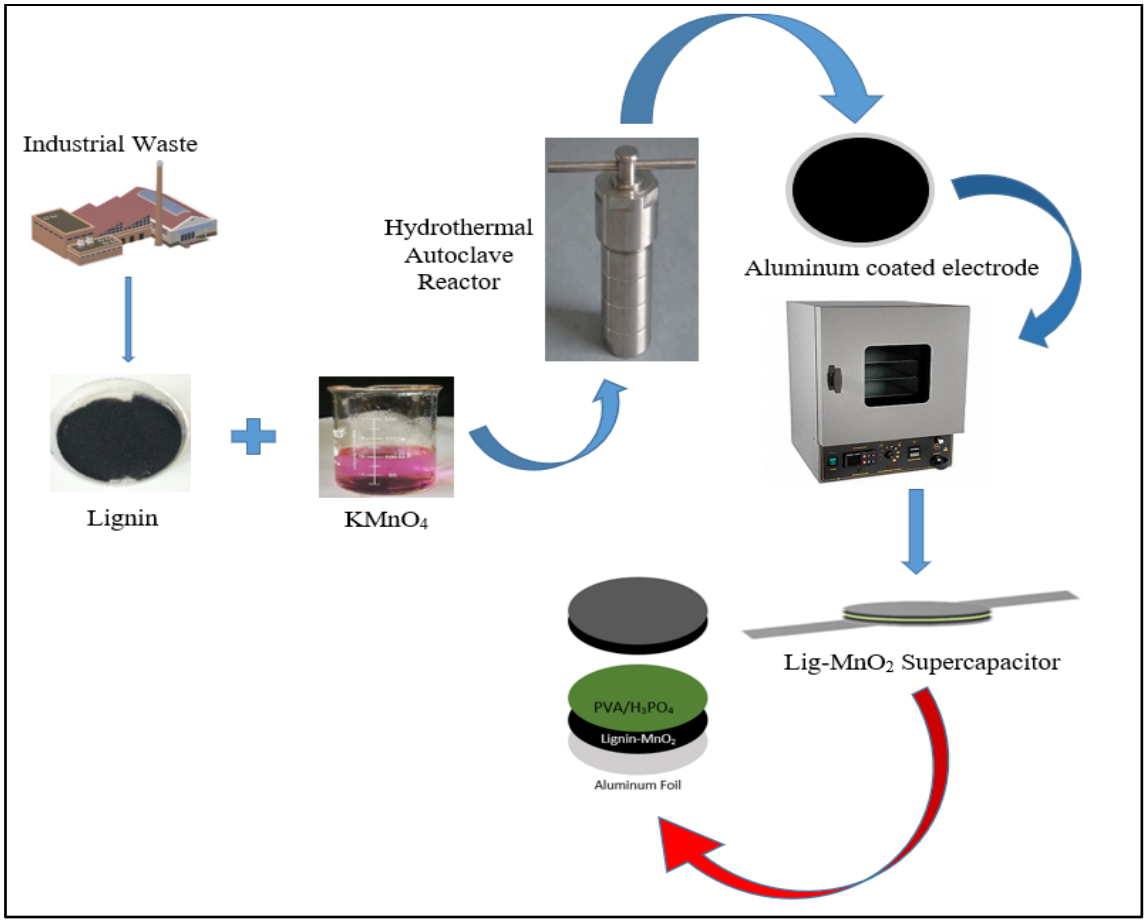

Figure 3.1: Schematic Process of Solid-state Asymmetric Supercapacitor

3.4. Materials Characterization

Scanning electron microscope (SEM) characterization was carried out to study the surface characteristics of the electrodes, the gel electrolyte, and the supercapacitor interface. For this, the VEGA/TESCAN model SEM, at the Texas A&M Mechanical Engineering Facility, was used. It employed an electron beam accelerated to 5 kV and provided a magnification of 100x.

3.5. Electrochemical Experiments

A Gamry potentiostat version 6.33 was used to perform the electrochemical characterization. For the cyclic voltammetry (CV) experiment, the Lignin-MnO_2 based electrode of the supercapacitor was used as the working (positive) electrode, and the reference and counter electrode terminals were connected to the AC based electrode of the supercapacitor.

To analyze the effect of scan rate voltage on the electrochemical performance of the supercapacitor, the CV experiment was carried out. In order to study the impedance behavior of the supercapacitor, electrochemical impedance spectroscopy (EIS) was also carried out at the frequency range of 10^6 Hz to 0.1 Hz, AC volts of 10 mV and DC at 1 V. The frequency range was selected so that all the important steps namely ion-transfer resistance in the electrolyte, charge transfer resistance in the capacitive double layer, which is high frequency-dependent phenomena, could be studied along with the low-frequency dependent diffusion kinetics in the electrode. Nyquist plots were obtained at regular intervals starting at the beginning, and after the end of the 260^{th}, 570^{th}, 1350^{th}, and the 2000^{th} cycle. The cyclic charge-discharge (CCD) experiment was run for 3000 cycles at a current density of 40 mAg^{-1} using a Gamry potentiostat. One-minute duration was provided each for a charge and discharge cycle.

3.5.1. Morphology Characteristics

In order to study the morphological characteristics, samples were analyzed using a Scanning Electron Microscope (SEM). It was used to observe the electrode-electrolyte

interface and surface features. Figure 3.2(a) shows the SEM images of the PVA/H_3PO_4 based gel electrolyte used in the supercapacitor interface. The surface of the electrolyte appears to be smooth and undamaged.

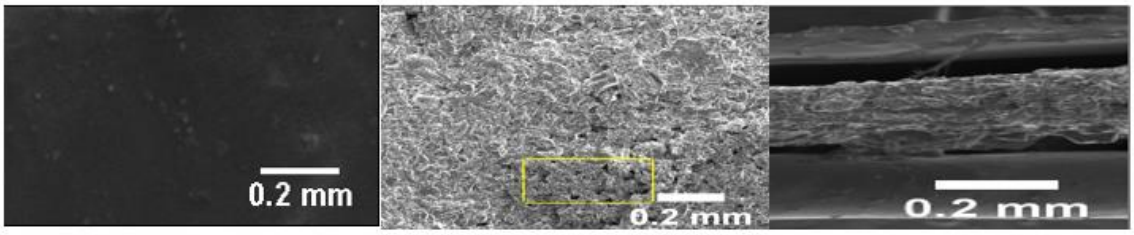

Figure 3.2: The high-resolution Scanning Electron Microscopic image of (a) the PVA/H_3PO_4 gel electrolyte, (b) the AC coated electrode, and (c) the supercapacitor interface showing the gel electrolyte sandwiched between electrodes with an outer Al current collect or layer at a scale bar = 0.2 mm.

This smooth electrolyte surface ensures there is good interfacial contact with the electrode surface and no undesirable reaction products are generated due to any impurity. In Figure 3.2(b), the surface of the negative electrode shows the AC particles evenly distributed throughout the electrode surface. The substrate used was Al foil. An even distribution of AC particles ensures better attachment and a higher contact area with the electrolyte. The particles appear clustered in some local regions and elongated. There are also seen regions with high porosity as shown in the yellow rectangle in Figure 3.2(b). The highly porous structure ensures a higher contact area for surface reaction. Figure 3.2(c) shows the supercapacitor interface. The electrolyte gel layer is sandwiched between the outer electrodes. The interface thickness is close to 100 microns. While, the attachment between the active material of the electrodes and the electrolyte layer is good, the attachment

between the active electrode material and the outer Al substrate seems weak. Also, the thickness of the electrode and the electrolyte seems non-uniform. The interface is mechanically stable, and the two electrode surfaces are congruent with the electrolyte. This provides a good condition for the electrochemical experiment. The attachment of the layers and uniformity of thickness can both be improved with more stringent process design and assembly.

3.5.2. Electrochemical Capacitive Performance

To test the electrochemical performance of the supercapacitor both cyclic voltammetry (CV) and cyclic charge-discharge (CCD) experiments are performed. In the CCD experiment, the supercapacitor was run for 3000 cycles at the current density of 40 mAg^{-1}. The comparison of the results from these two experiments gives a holistic picture of the electrochemical behavior of the supercapacitor.

3.5.2.1. Cyclic Voltammetry (CV) Test

After running CV tests for various voltage ranges at 100 mVs^{-1}, and at various scan rates (5, 10, 25, and 50 mVs^{-1}) the voltage range of 1-2V at a scan rate of 10 mVs^{-1} was selected for further testing. The comparative CV plots for the voltage ranges and scan rates are shown in Figure 3.3.

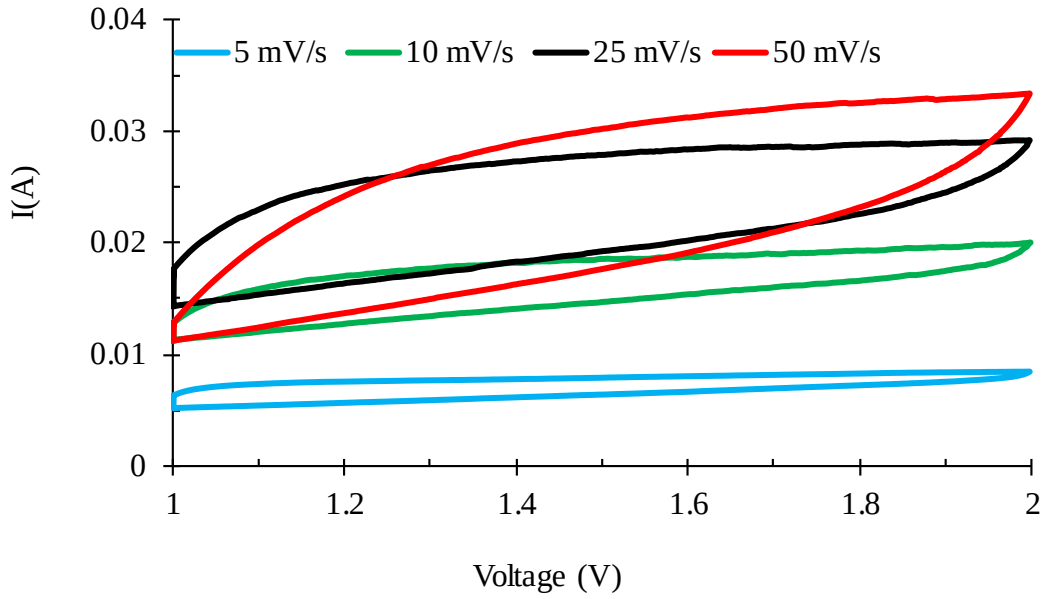

(a)

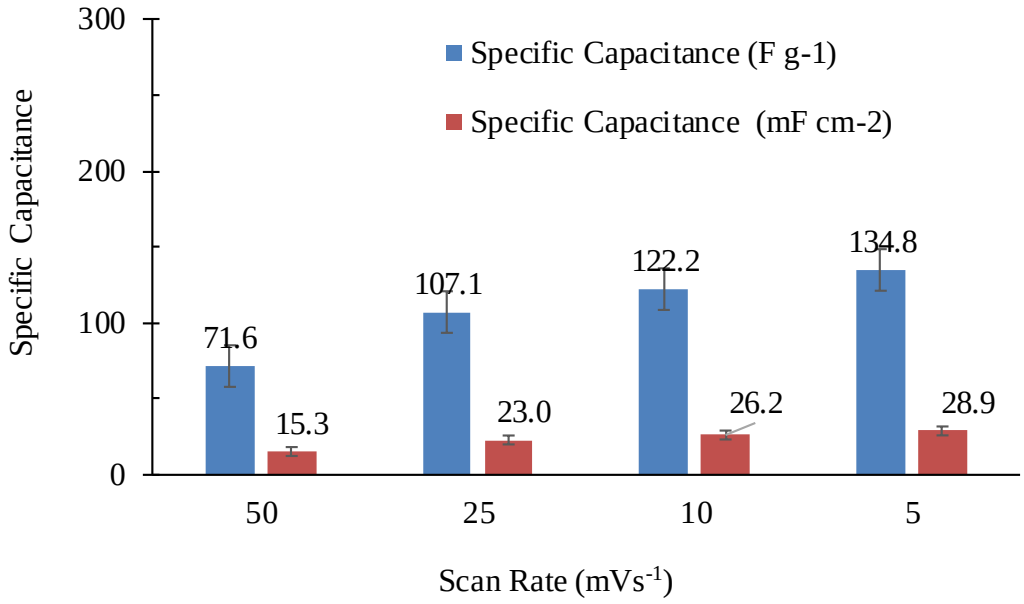

(b)

Figure 3.3: (a) Cyclic voltammetry curve of lig- MnO2 supercapacitor at various scan rates: 5 (sky blue), 10 (green), 25 (black), and 50 mVs-1 (red), (b) comparative histogram of specific capacitance versus scan rate, (c) cyclic voltammetry curves for different vo voltage ranges, and (d) comparative histogram of specific capacitance versus voltage range at 10 mVs-1.

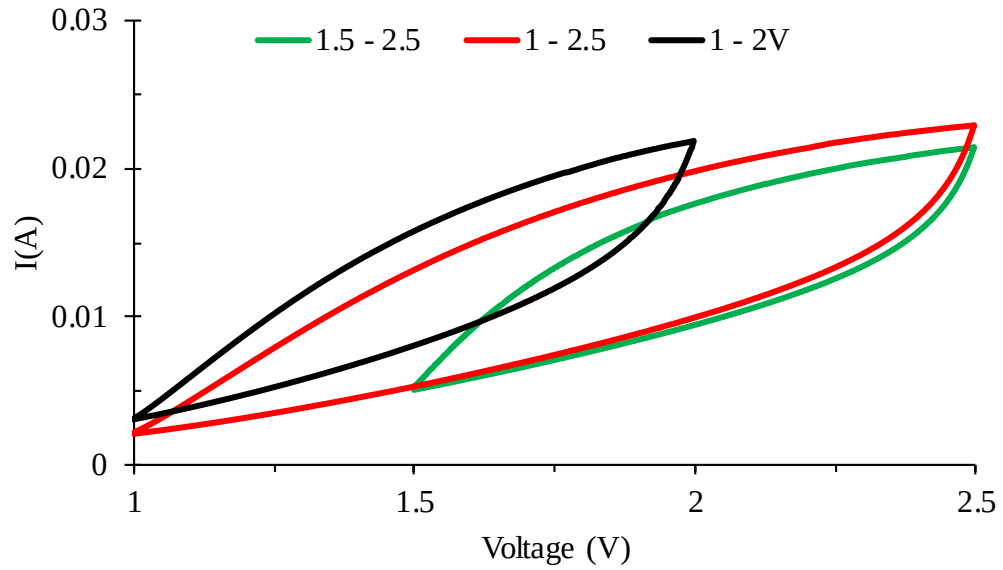

(c)

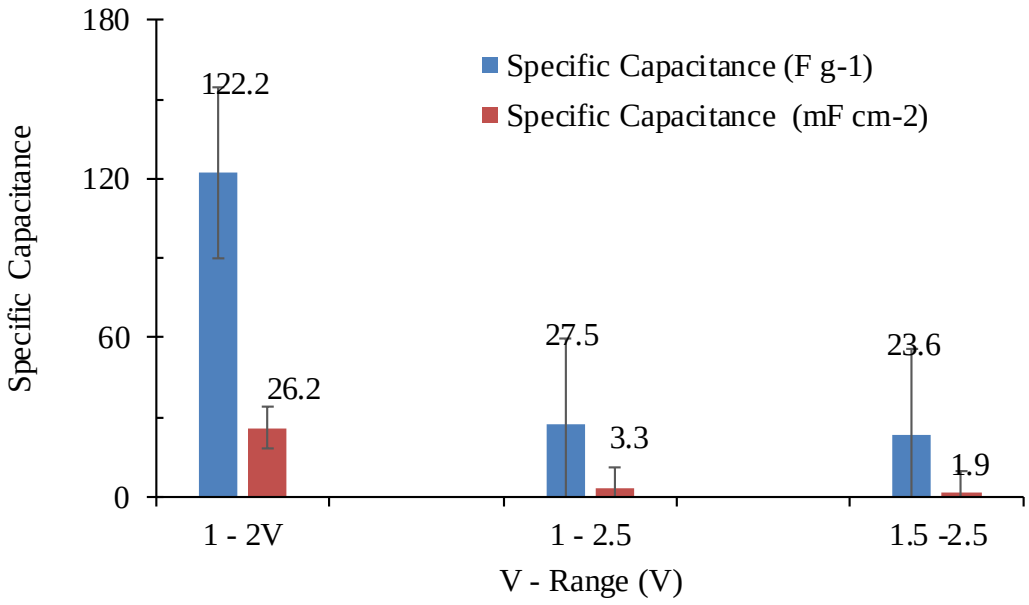

(d)

Figure 3.3 Continued

For comparison, the CV curves obtained at scan rates 5, 10, 25, and 50 mVs^{-1} are shown in Figure 3.3 (a). The CV characteristics are better at 10 mVs^{-1} than at 5 mVs^{-1}/100 mVs^{-1} which can be seen by a more rectangular-shaped curve at 10 mVs^{-1}. At scan rates higher than 10 mVs^{-1}, the scan voltage rate is too fast while for scan rate lower than 5 mVs^{-1}, it is too slow for stable system dynamics. Thus, an ideal scan rate of 10 mVs^{-1} was selected to perform the cyclic voltammetry for longer runs. This fact is also evidenced by the specific capacitance obtained at varying scan rates as shown in Figure 3.3(b). The average value of specific capacitance for the supercapacitor obtained at 10 mVs^{-1} is 122.21 Fg^{-1} (26.19 $mFcm^{-2}$) which is the highest while that obtained at 50 mVs^{-1} is 71.58 Fg^{-1} (15.34 $mFcm^{-2}$) which is the least. It is also important to ascertain the operating voltage window for the cyclic voltammetry experiment. Cyclic voltammetry curves were obtained accordingly for several voltage windows (Figure 3.3(c)). Figure 3.3(d) shows the obtained specific capacitances at several voltage ranges for a scan rate of 10 mVs^{-1}. It is seen that we obtain the highest average specific capacitance in the voltage range of 1-2V (122.21 Fg^{-1}) and the least in the voltage range 1.5 – 2.5 V (23.59 Fg^{-1}).

3.5.2.2. Cyclic Charge-Discharge (CCD) Test

The cyclic charge-discharge experiment was carried out for 3000 cycles at a current density of 40 mA g^{-1}. The variation of specific capacitance with cycles for the cyclic charge-discharge experiment is shown in Figure 4a. The y-axis is shown in log scale. The decline of specific capacitance can be observed as the number of cycles increase. However, this decline is very slow. The maximum value of the specific capacitance was

about 379.06 mF cm^{-2} at the first cycle while the minimum value was about 298.17 mF cm^{-2} at the 3000th cycle.

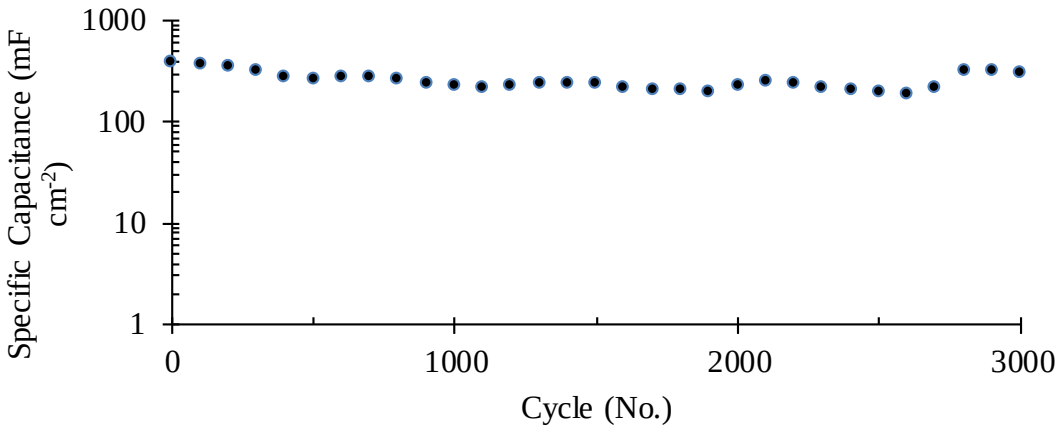

Figure 3.4: Variation of specific capacitance at a current density of 40 mAg^{-1} for 3000 cycles (CCD test)

The cyclic charge-discharge experiment was carried out for 3000 cycles at a current density of 40 mA g^{-1}. The variation of specific capacitance with cycles for the cyclic charge-discharge experiment is shown in Figure 3.4. The y-axis is shown in log scale. The decline of specific capacitance can be observed as the number of cycles increase. However, this decline is very slow. The maximum value of the specific capacitance was about 379.06 mF cm^{-2} at the first cycle while the minimum value was about 298.17 mF cm^{-2} at the 3000th cycle. The supercapacitor shows significantly high values of specific capacitance over a wide range of 3000 cycles in the voltage window of 1V which has many practical applications. The gradual decline in the specific capacitance can be attributed to the use of unprocessed lignin.

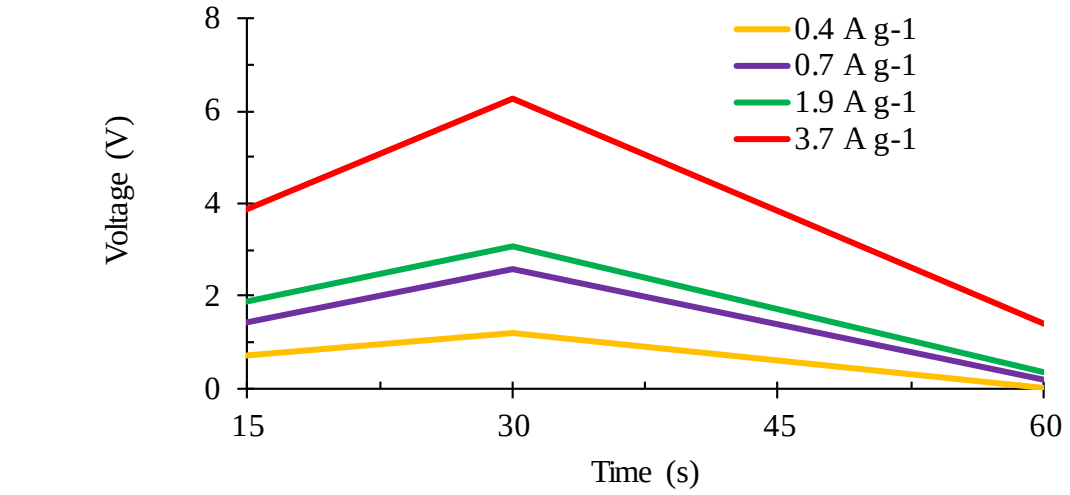

(a)

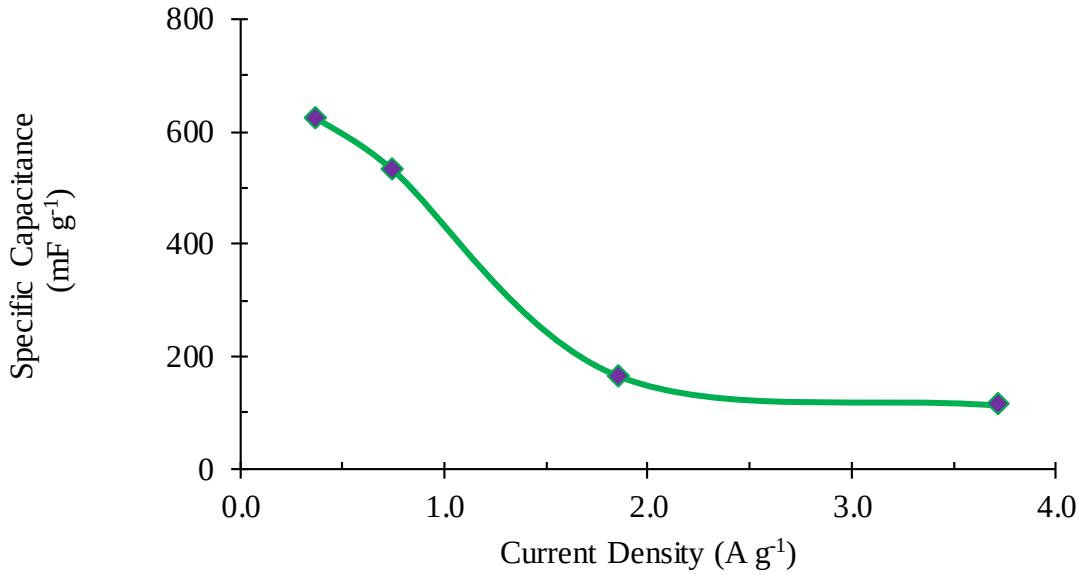

(b)

Figure 3.5: Comparative plots of (a) voltage versus time at different current densities, and (b) specific capacitance versus current density in the cyclic charge-discharge experiment at a charge current of 1 mA. (c) Plots of energy density (black) and power density (red) versus cycles for the lig-MnO2 supercapacitor in CCD experiment, and (d) Ragone plot of the lig-MnO2 supercapacitor.

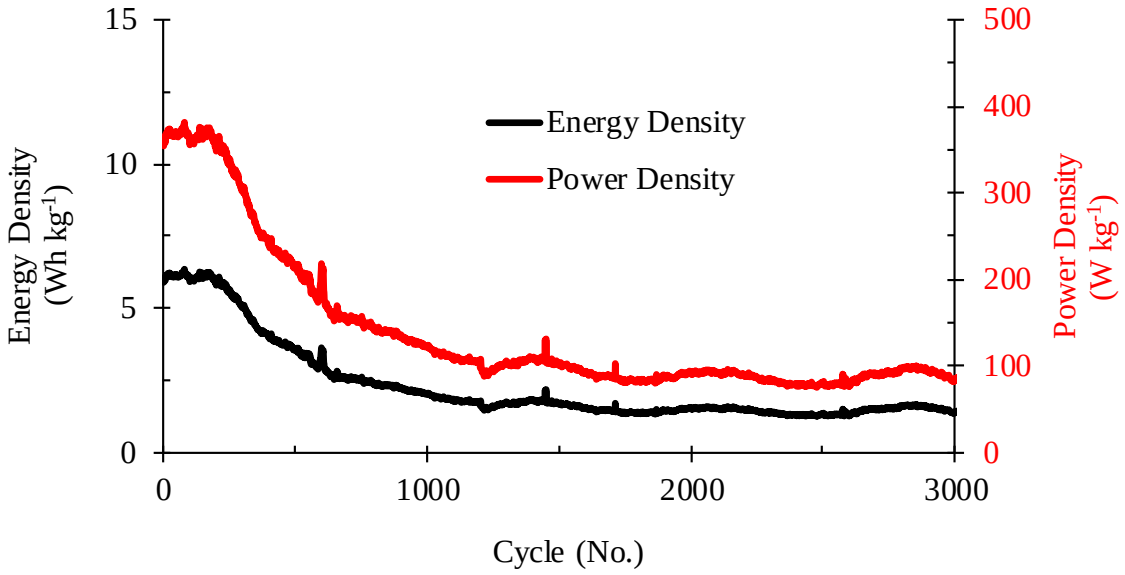

(c)

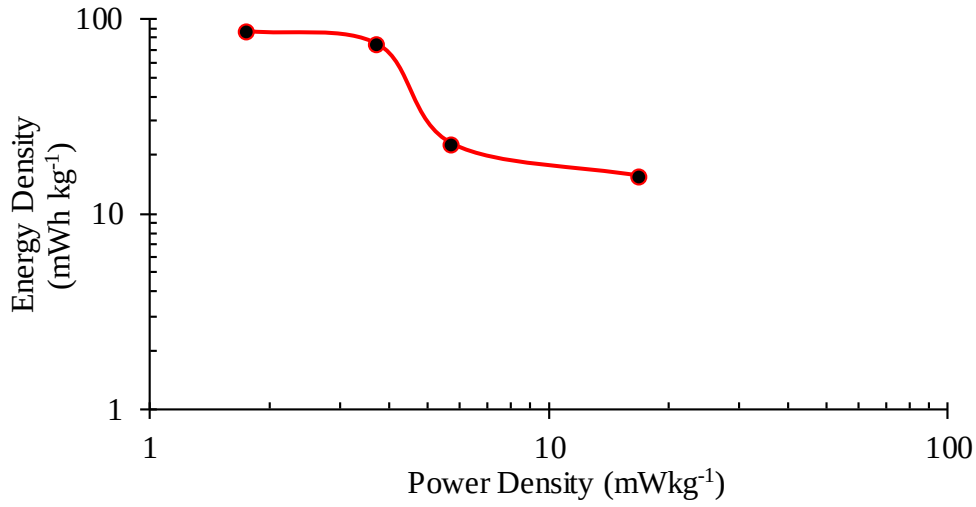

(d)

Figure 3.5 Continued

To observe the impact of current density on the resultant discharge voltage in the cyclic charge-discharge experiment, Figure 3.5(a) is obtained. The resultant voltage curves are obtained at various current densities of 0.4 Ag^{-1} (orange), 0.7 Ag^{-1} (purple), 1.9 Ag^{-1} (green), and 3.7 Ag^{-1} (red). At varying current densities, the rate of decline (slope) of the

discharge voltage curves is observed. Higher the current density steeper is the slope of the voltage-time curve. Thus, at higher current density the voltage drop is at a higher rate. To obtain the effect of discharge current density on specific capacitance, Figure 3.5(b) is obtained for a constant charge current of 1 mA. Specific capacitance declines with increasing discharge current density. This behavior is reflective of any supercapacitor.

To obtain the energy and power characteristics of the supercapacitor, the energy density (black) and power density (red) curves are obtained and shown in Figure 3.5(c). The energy density and the power density both decrease with cycle number, and the decrease is gradual. Energy density of ~6 Wh kg^{-1} is obtained initially and ~1.5 Wh kg^{-1} at the end of 3000 cycles. Consistency in energy density can be observed throughout after an initial drop at about the 1000^{th} cycle. The initial power density obtained is ~355 W kg^{-1}, which declines to ~100 W kg^{-1}after 3000 cycles. Similar to energy density, the power density is fairly consistent after the 1000^{th} cycle. Even though there is a gradual decline in both the energy and power densities, which may be attributed to the simplistic nature of the supercapacitor assembly and design and the use of unprocessed lignin.

A Ragone plot (Figure 3.5(d)) is shown for the supercapacitor which shows the variation of the energy density with the power density at varying current densities as obtained from the cyclic charge-discharge experiment. The nature of the curve is consistent with those reported for MnO_2 based supercapacitors.

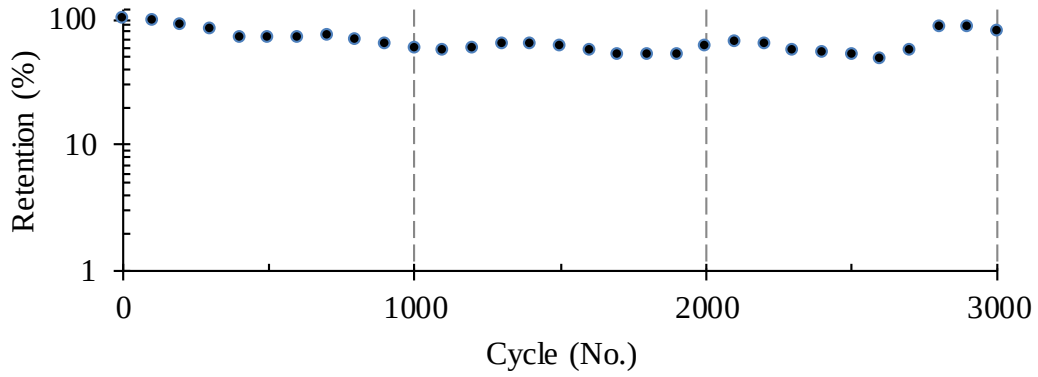

Figure 3.6: Capacitance retention for the lig-MnO2 supercapacitor (CCD experiment) for the 3000 cycles

For the CCD experiment, the capacitance retention for the supercapacitor is calculated and the retention % is plotted for 3000 cycles accordingly in Figure 3.6. The capacitance retention declines from an initial value of 100 % to about 80 % after 3000 cycles. The trend of retention is non-monotonic. For every 1000 cycles interval, the first interval shows a progressive decline, the second shows consistency, while the last interval shows a slow rise. Thus, a threshold value of specific capacitance, and corresponding energy and power densities, can be easily determined (using the value at the start of the last interval, i.e. at the 2000^{th} cycle) at which the supercapacitor can be used with ~ 98 % retention for the entire 3000 cycles for many electronic devices which operate within that specific capacitance range. This retention behavior may work well with devices that require variable power or energy after some usage.

3.5.2.3. Electrochemical Impedance Spectroscopy (EIS)

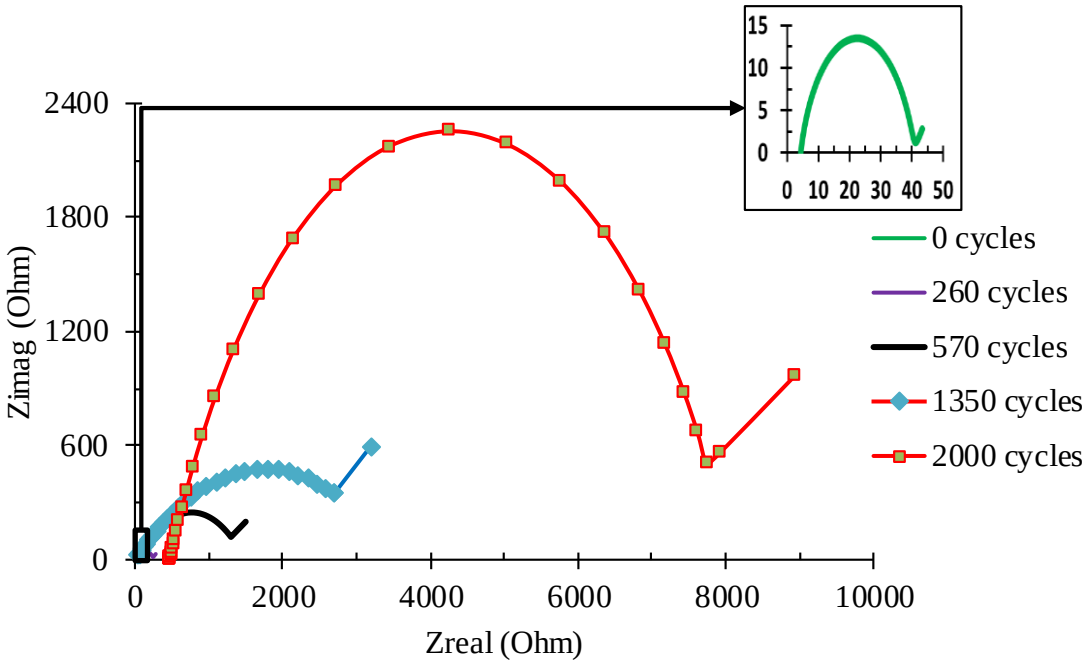

Figure 3.7: Electrochemical impedance spectroscopy (Nyquist plots)

Electrochemical impedance spectroscopy (EIS) was carried out to study the impedance behavior of the supercapacitor, and accordingly, the Nyquist plots are obtained (Figure 3.7). From the plot, the total impedance after the 260th cycle (purple) is calculated to be 102 ohm which is greater than the value at the beginning (green). The impedance values keep increasing as the number of cycles increase. This indicates that with the progression of cycles, the resistance to current flow increases, and hence it results in a lesser current flow and lesser capacity retention towards higher cycle numbers. The rate at which impedance develops is relatively slow in the beginning, and then steeps rapidly. A considerable increase of impedance beyond the 1350th cycle leads to a decline in retention of capacitance. This may be due to the buildup of complex reaction products altering the

speed of electron transport in the material as well as the possibility of material undergoing morphology change or phase transformation at the microstructure level, resulting in slower movement of electrons, thereby increasing the bandgap of conduction.

3.6. Summary

A solid-state asymmetric supercapacitor was assembled, with the active material for the working electrode as lignin decorated with MnO_2 particles and for the counter electrode was AC. The electrolyte used was PVA/H_3PO_4. Via the SEM imaging, the interface is found to be mechanically stable, and the two electrode surfaces conform with the electrolyte. The CV test was used to determine the ideal voltage range (1 - 2 volts) and scan rate (10 mV s^{-1}) for the supercapacitor. The CCD test shows the system stability and retention. The highest specific capacitance obtained was 379.06 mF cm^{-2} at the first cycle while the minimum value was about 298.17 mF cm^{-2} at the 3000^{th} cycle with ~ 98% retention. EIS shows the impedance behavior of the supercapacitor.

4. MNO_2 DECORATED, ACTIVATED CARBON & LIGNIN BASED NOVEL ELECTRODES

In the earlier chapter we studied the capacitive performance of the electrode made from the lignin, decorated with a transitional metal oxide (MnO_2) particles. In this chapter, lignin is combined with another biomaterial, Activated Carbon (AC) and decorated with MnO_2 particles. The effect of AC combined with lignin and the differences in performance have been analyzed using three electrochemical tests; Cyclic Voltammetry (CV), Cyclic Charge-Discharge (CCD) and Electrochemical Impedance Spectroscopy (EIS).

4.1. Preparation of AC/lignin/MnO_2 Composite Electrode

First, a 50 ml $KMnO_4$ solution of 47.5µmol was made. Then 0.3 g of alkaline lignin powder and 0.2 g activated carbon were mixed in the ratio 3:2 by weight to obtain a mixture of AC and lignin. Hydrothermal treatment was carried out at 160^0 C for 1 hour after which, the excess liquid was drained. The resulting slurry was dried in a vacuum oven overnight at 60^0C. The powder obtained was mixed with PVDF in the ratio 4:1, and 2 ml of NMP was added to the slurry. The slurry was coated on an aluminum foil substrate cut in the form of a circular plate of diameter 4 cm. The adjoining strips of the foil were 1 cm wide and 3 cm long. The coated foil was heated in a vacuum oven for 4 hours at 100°C to obtain the AC/lignin/MnO_2 composite electrode.

4.2. Preparation of PVA/H_3PO_4 Gel Electrolyte

The method for the preparation of the electrolyte has been mentioned in chapter 3, section 3.2. No details will be repeated here.

4.3. Assembly of Solid-state Asymmetric Supercapacitor

As mentioned in chapter 3, section 3.3. The assembly of this solid-state supercapacitor is shown in Figure 4.1.

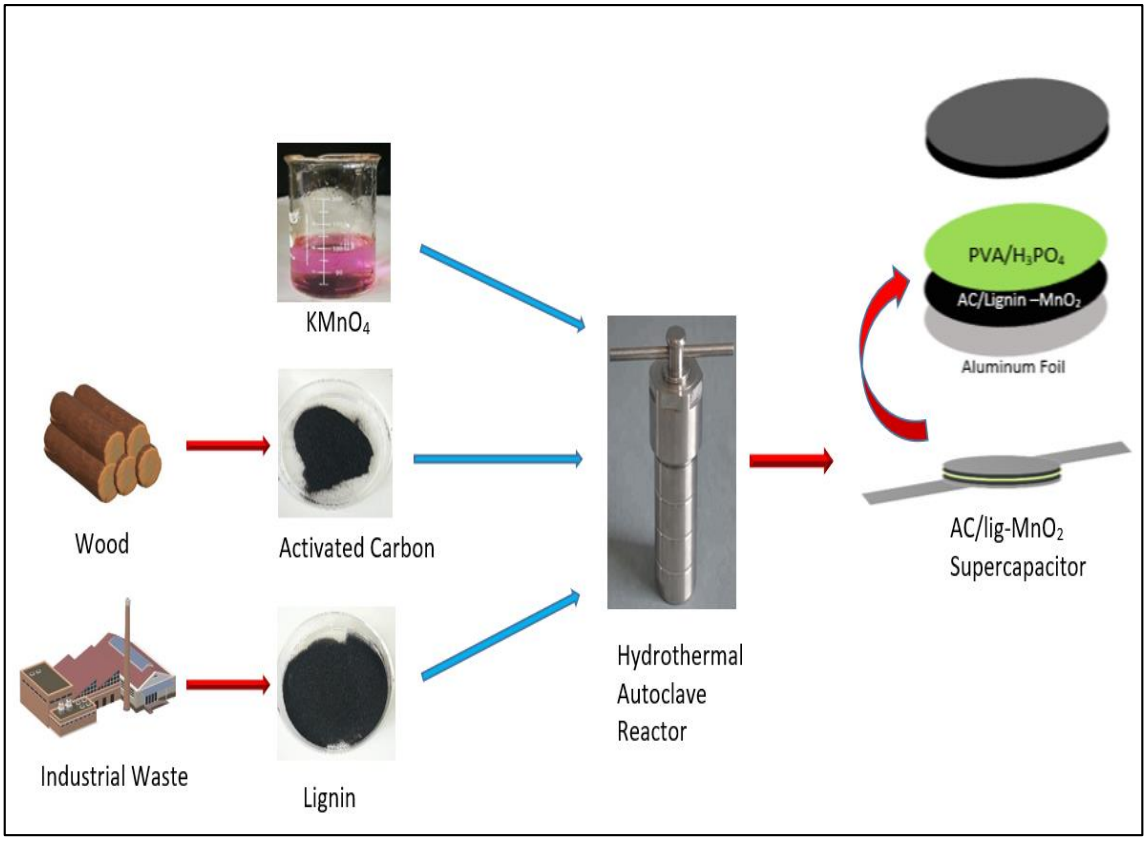

Figure 4.1: Schematic Process of Solid-state Asymmetric Supercapacitor

4.4. Materials Characterization

The characterization methods have been described in Chapter 3, section 3.4. No details will be repeated here.

4.5. Electrochemical Experiments

The electrochemical experiments have been explained in chapter 3, section 3.5. No details will be repeated here.

4.5.1. Morphology Characteristics

Morphology of the samples was studied using SEM. It was used to observe the electrode-electrolyte interface and surface features. Figure 4.2(a) shows the SEM images of the PVA/H_3PO_4 based gel electrolyte used in the supercapacitor interface. We see that the surface of the electrolyte appears to be smooth and without any damage. This smooth electrolyte surface ensures there is good interfacial contact with the electrode surface and no unwanted reaction products are generated due to undesirable side reactions due to any impurity. In Figure 4.2(b) we see the negative electrode surface showing AC particles. The AC particles are seen evenly distributed throughout the electrode surface. The substrate used was Al foil. An even distribution of AC particles ensures better attachment and higher contact area with the electrolyte. The particles appear clustered in some local regions and elongated. There are also seen regions with high porosity as shown in the yellow rectangle in Figure 4.2(b). The highly porous structure is helpful for higher contact area for surface reaction.

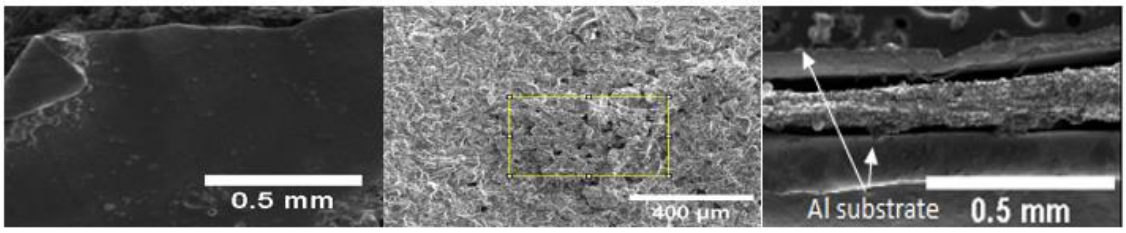

Figure 4.2: High-resolution Scanning Electron Microscope image of (a) the PVA/H_3PO_4 gel electrolyte; scale bar =0.5 mm, (b) the AC coated electrode, scale bar =400 µm, and (c) supercapacitor interface showing gel electrolyte sandwiched between electrodes with outer Al current collector layer, scale bar =0.5 mm.

Figure 4.2(c) shows the supercapacitor interface. The electrolyte gel layer is sandwiched between the outer electrodes with Al as the substrate. The interface thickness is close to 100 microns. The active material of the electrodes seems well attached to the electrolyte layer. However, the attachment between the active electrode material and the outer Al substrate seems weak. Also, the thickness of the electrode and the electrolyte seems non-uniform. The interface is mechanically stable, and the two electrode surfaces are congruent with the electrolyte. This provides a good condition for the electrochemical experiment. The attachment of the layers and uniformity of thickness can both be improved with more stringent process design and assembly. To understand the morphology of particles of the AC/lignin matrix, it is simpler to first analyze them in separate set up. Corresponding to this, two separate fresh samples of supercapacitors were assembled for experimenting; one made up of AC, and the other of lignin.

4.5.2. Electrochemical Capacitive Performance

To test the electrochemical performance of the supercapacitor both cyclic voltammetry (CV) and cyclic charge-discharge (CCD) experiments were performed. In the CV experiment, we cycle the supercapacitor keeping the voltage window (1-2 Volts) and scan rate (10 mV s^{-1}) constant for 2000 cycles, while in CCD experiment, we keep the current density (6.01 mAg^{-1}) constant for 2000 cycles. The comparison of the results from these two experiments gives a holistic picture of the electrochemical behavior of the supercapacitor.

4.5.2.1. Cyclic Voltammetry (CV) Test

For comparison, the CV curves obtained at scan rates 5, 10, 25, and 100 mVs^{-1} are shown in Figure 4.3(a). The CV characteristics are better at 10 mVs^{-1} than at 5 mVs^{-1} or 100 mVs^{-1} which can be seen by a more rectangular-shaped curved at 10 mVs^{-1}. At scan rates higher than 10 mVs-1, the scan voltage rate is too fast while for scan rate lower than 5 mVs^{-1}, it is too slow for a stable system dynamic. Thus, the ideal scan rate is 10 mVs^{-1} which is selected to perform the cyclic voltammetry for longer runs. This fact is also evidenced by the specific capacitance obtained at varying scan rates and shown in Figure 4.3(b).

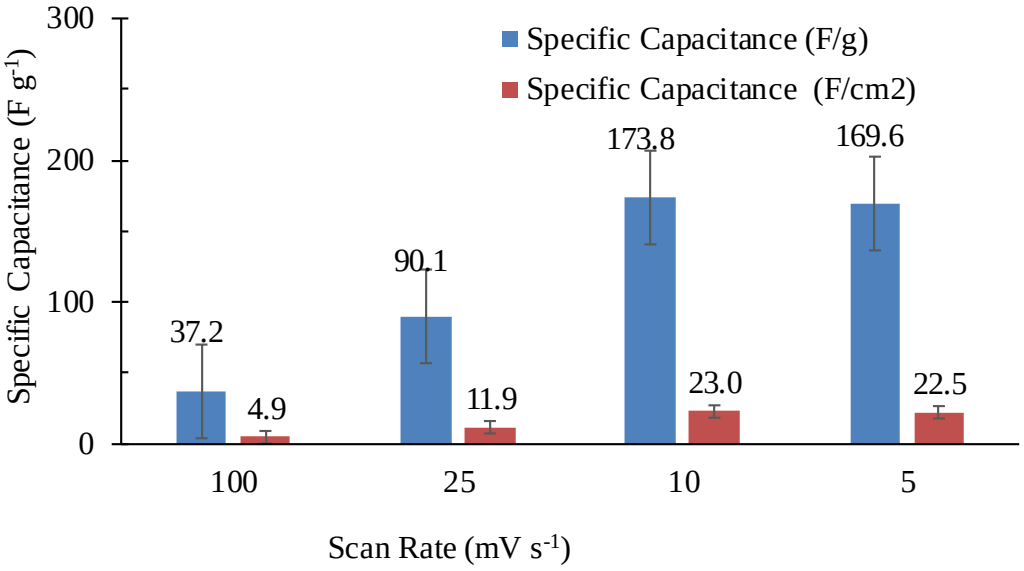

(a)

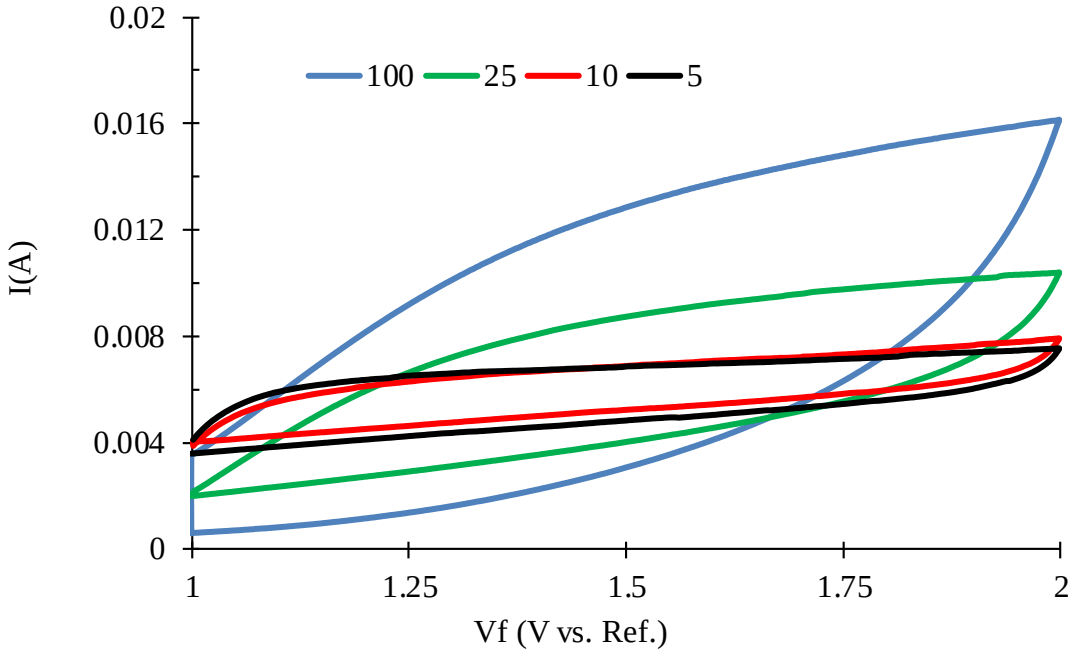

(b)

Figure 4.3: (a) Cyclic voltammetry curve of AC/lig- MnO_2 supercapacitor at various scan rates: 5 (black), 10 (red), 25 (green), and 100 mVs^{-1} (blue), (b) comparative histogram of specific capacitance versus scan rate, (c) comparative histogram of specific capacitance versus voltage range at 10 mVs^{-1}

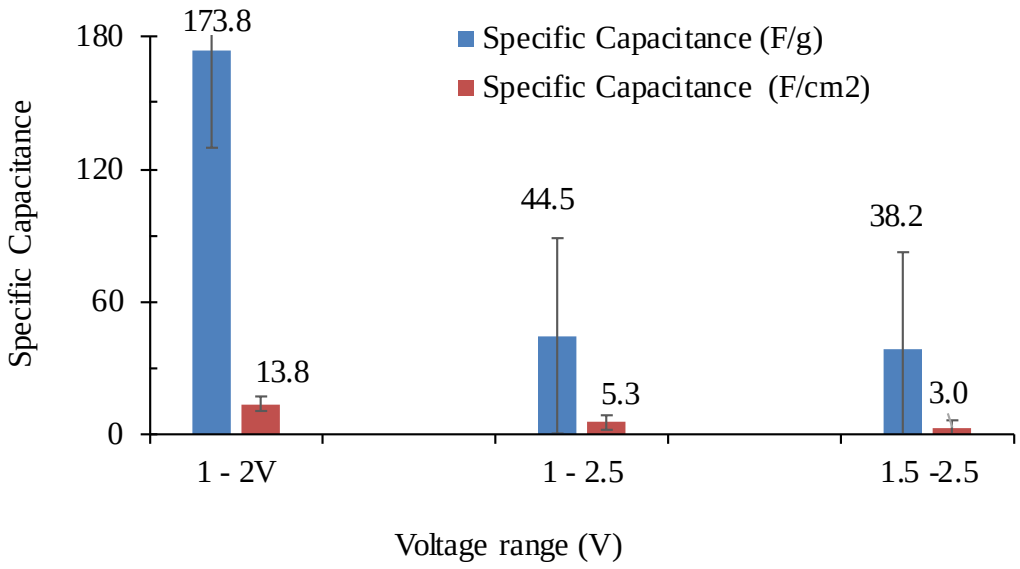

(c)

Figure 4.3 Continued

The average value of specific capacitance for the obtained at 10mVs^{-1} is 173 Fg^{-1} (23.01 mFcm^{-2}) which is the highest while that obtained at 100 mVs^{-1} is 37.16 Fg^{-1} (4.92 mF cm^{-2}) which is the least. It is also important to ascertain the operating voltage window for the cyclic voltammetry experiment. Figure 4.3(c) shows the obtained specific capacitances at several voltage ranges for a scan rate of 10 mVs^{-1}. It is seen that we obtain the highest average specific capacitance in the voltage range of 1-2V.

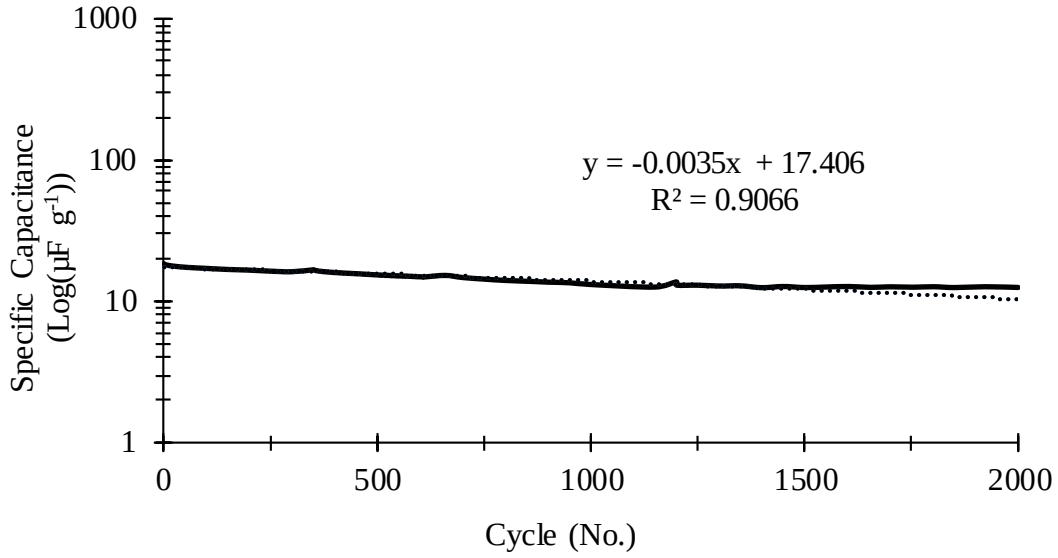

Figure 4.4: Variation of specific capacitance with cycles for CV experiment for voltage range 1-2 V at 10 mVs^{-1}.

To study the electrochemical performance of the supercapacitor using cyclic voltammetry, the specific capacitance versus cycle plot was obtained, shown in Figure 4.4. A log plot is obtained so as to get a more insightful detail of the specific capacitance variation. The plot is fit with a regression equation shown on the plot. The fit is a simple linear line with a negative slope of (-0.0035) and intercept of 17.4. A very high value of the coefficient of determination, R^2 (0.91), indicates that the simple linear line model fits perfectly well. The negative slope of the curve indicates that, overall, the specific capacitance depreciates with cycles. However, since the value of the slope is very small, it means that the rate of decrease of the specific capacitance is relatively small. Nevertheless, the specific capacity of the supercapacitor, which is 173.8 Fg^{-1} (23 $mFcm^{-2}$) initially and 35 mFg^{-1} (2.8 $mFcm^{-2}$) at the end of 2000 cycles, varies considerably towards the end of 2000 cycles. This is to be expected for this simplistic design and assembly process. The supercapacitor is able to

deliver significantly high values of specific capacitance over a wide range of 2000 cycles and voltage window of 1V which is practical for many applications in general. Even though there is a gradual decline in the specific capacity, which may be due to the use of unprocessed lignin, the value is comparable to those reported in the literature[47]. This shows the viability of this device for numerous applications in the specified specific capacitance range of 173.8 Fg^{-1} to 35 mFg^{-1}. The electrochemical performance comparison for the exact same material (lignin-MnO_2), in this case, is not possible since it is a new material.

4.5.2.2. Cyclic Charge-Discharge (CCD) Test

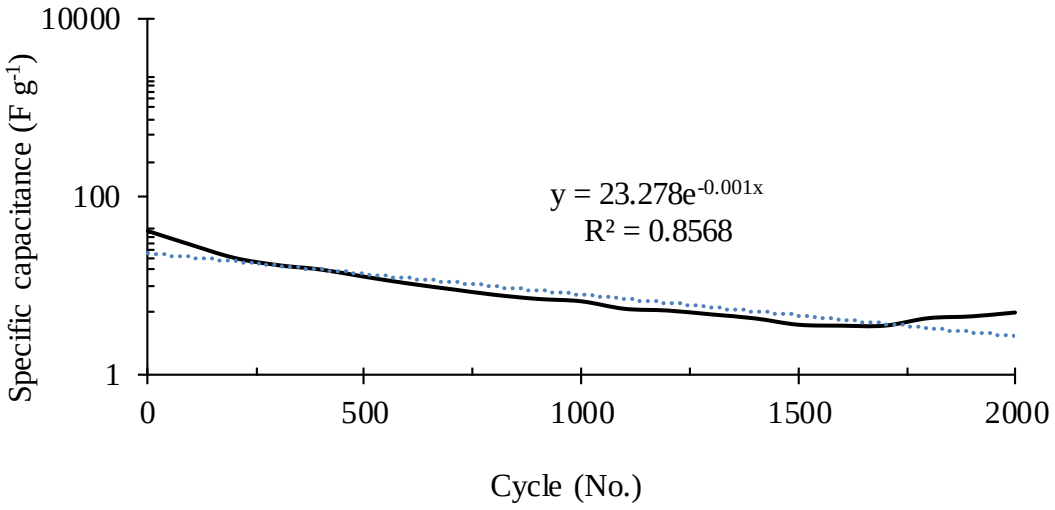

Figure 4.5: Variation of specific capacitance with cycles for CCD experiment at a current density of 6.01 mAg^{-1} for 2000 cycles

Cyclic charge-discharge experiment was carried out at a current density of 6.01 mAg^{-1}. The variation of specific capacitance with cycles for the cyclic charge-discharge

experiment is shown in Figure 4.5. The y-axis is shown in log scale. The experiment is run for 2000 cycles. The specific capacitance seems to decline with the number of cycles. However, this decline is very slow and closely resembles an exponential decay equation with a pre-exponential factor of 23.27 and the argument of the exponent is -0.001. The coefficient of determination for this fit is 0.85 which shows a relatively good fit of the decay curve with this model equation. The maximum value of the specific capacitance is ~ 41.23 Fg^{-1} at the first cycle while the minimum value is ~ 5 Fg^{-1} at the 2000^{th} cycle. The value of specific capacitance obtained is high relative to many other similar supercapacitors reported in the literature, and well suited for many applications [47].

To observe the impact of current density on the resultant discharge voltage in the cyclic charge-discharge experiment, Figure 4.6(a) is obtained. The resultant voltage curves are obtained at various current densities of 1.2 mA/g (yellow), 3.01 mA/g (purple), 6.01 mA/g (green) and 9.01 mA/g (red). The key point of interest here is the rate of decline (slope) of the discharge voltage curves at varying current densities. It is seen that the higher the current density steeper is the slope of the voltage-time curve.

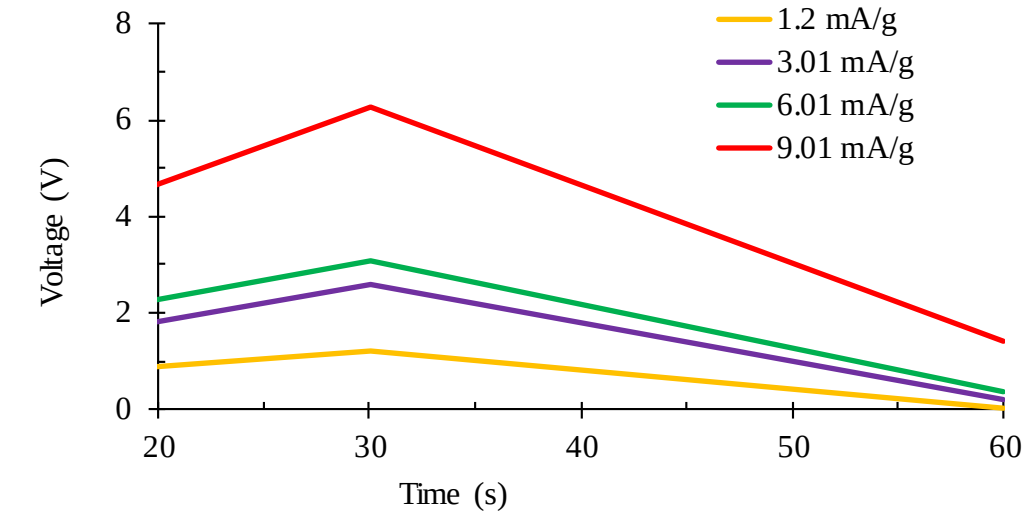

(a)

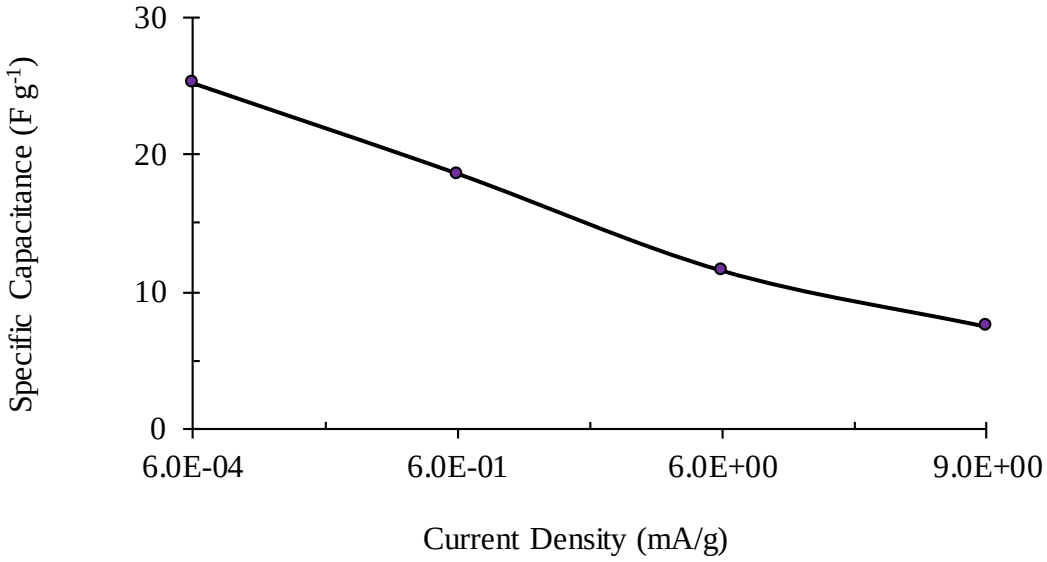

(b)

Figure 4.6: Comparative plots of (a) voltage versus time at different current densities, and (b) specific capacitance versus current density in the cyclic charge discharge experiment at a charge current of 2 mA

Thus, at higher current density the voltage drop is at a higher rate. This is expected behavior for any supercapacitor. To obtain the effect of discharge current density on specific capacitance, Figure 4.6(b) is obtained for a constant charge current of 2 mA. The

specific capacitance declines with increasing discharge current density. This too is reflective of the behavior of any supercapacitor.

For the CCD experiment at the current density of 6.01 mAg^{-1}, the retention % is plotted for the 2000 cycles for every interval of 500 cycles in Figure 4.7.

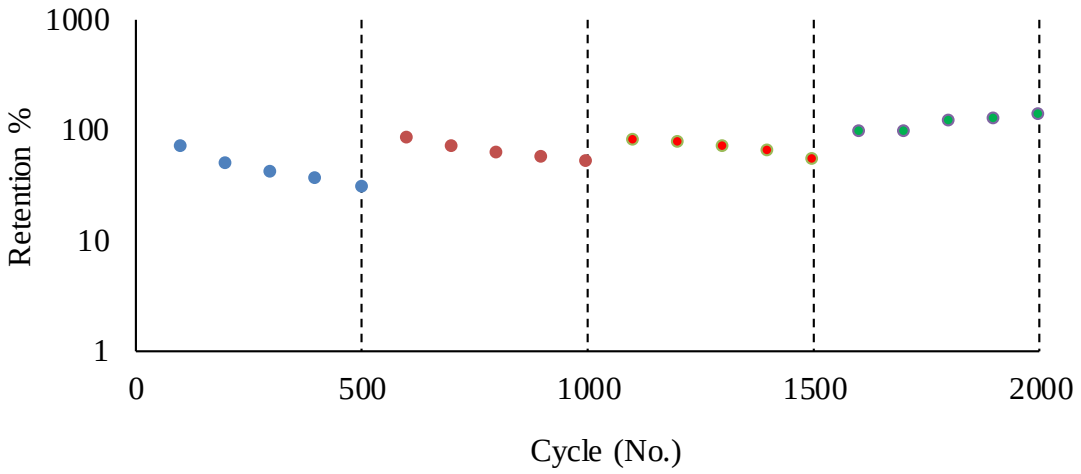

Figure 4.7: Capacitance retention plot for the AC/lig-MnO_2 supercapacitor in CCD experiment for the 2000 cycles

The starting value of capacitance at each interval is taken as reference for calculation of retention in any interval. For the first interval of 1-500 cycles, the retention gradually falls from an initial value of 80 % to 30 %. Similarly, for the second and third intervals of 500-1000 cycles and 1000-1500 cycles, the capacitance retention falls from about 84% to 52% and from 82% to about 54% respectively. For the fourth interval from 1500-2000 cycles, the retention goes up from about 97% to about 137% which is indicative of higher comparative stability. This shows that the supercapacitor has varied retention characteristics at various intervals. Also, the trend of retention is non-monotonic, the first

three intervals showing a progressive decline while the last interval shows a progressive rise. Thus, a threshold value of specific capacitance, and corresponding energy and power densities, can be easily determined (for the value at the start of the last interval i.e. at 1500th cycle) at which the supercapacitor can be used with ~ 99% retention for the entire 2000 cycles for many electronic devices which operate within that specific capacitance range. This retention behavior will also work well for devices having variable power or energy requirement after some usage.

4.5.2.3. Electrochemical Impedance Spectroscopy (EIS)

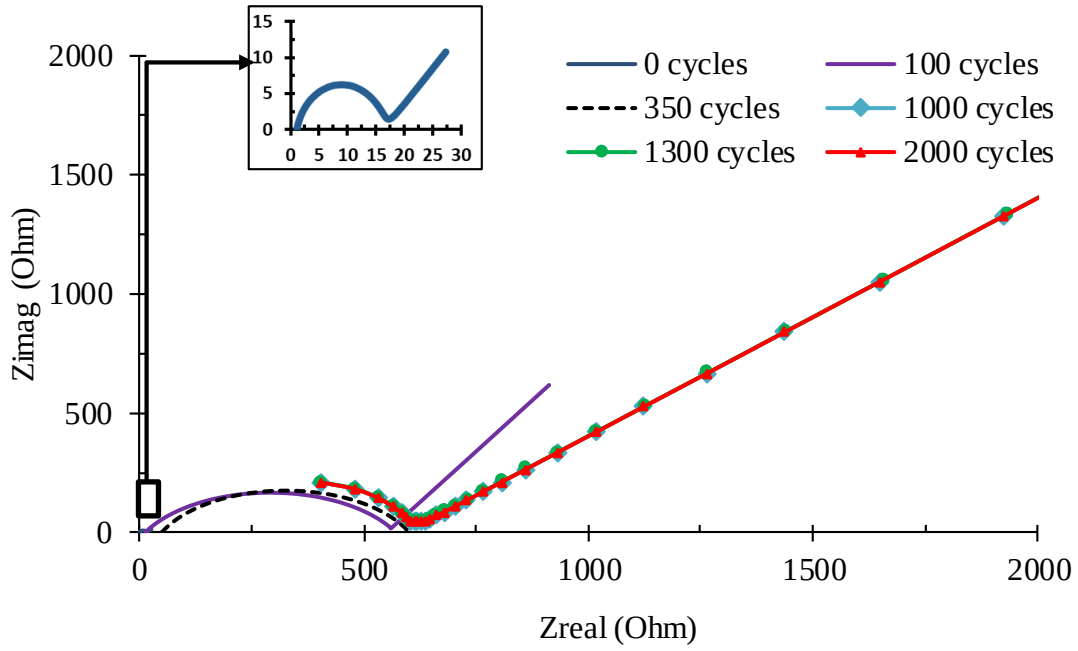

Figure 4.8: Electrochemical impedance spectroscopy (Nyquist plots)

Electrochemical impedance spectroscopy was carried out to understand the impedance behavior of the supercapacitor, and accordingly, the Nyquist plots are obtained and shown

in Figure 4.8. The total impedance after the 100th cycle (purple) is 558 ohm which is greater than 17.3 ohm, the value at the beginning (dark blue). Similarly, the impedance after the 350th cycle (dotted black) which is 593 ohms is greater than that after the 100th cycle. The impedance values after the 1000th, 1300th and 2000th cycles recorded were 613 ohms, 628 ohms, and 638 ohms respectively which are very close and differ only slightly. This indicates that after about 1000 cycles, the cumulative impedance of the electrolyte and the double layer capacitance hits a threshold value and the difference in current occurring is largely due to the kinetic diffusion resistance offered by the electroactive material. The impedance values follow the trend from the least to the greatest. This indicates that with the progression of cycles, the resistance to current flow increases, and it results in lesser current flow and lesser capacity retention as the cycle number increases. The rate at which impedance develops, however, is steeped in the beginning, and then declines rapidly from the 1000th to the 2000th cycle. Only a little increase of impedance beyond the 1000th cycle leads to the remarkable stability and retention of capacitance. This suggests some prominent physical or chemical change in the material after the 1000th cycle. A possible explanation could be the buildup of complex reaction products altering the speed of electron transport in the material. There could also be the possibility of material undergoing morphology change or phase transformation at the microstructure level, which aids in a faster movement of electrons, thereby reducing the bandgap of conduction.

4.6. Summary

A solid-state asymmetric supercapacitor was assembled, with the active material for the anode as a combination of AC and lignin, decorated with MnO_2 particles. The active material for the cathode was AC. The electrolyte used was PVA/H_3PO_4. Via the SEM imaging, the interface is found to be mechanically stable, and the two electrode surfaces conform with the electrolyte. The CV test was used to determine the ideal voltage range (1- 2 volts) and scan rate (10 mV s^{-1}) for the supercapacitor. The CCD test shows the system stability and retention. The highest specific capacitance obtained is ~ 41.23 Fg^{-1} while the minimum value is ~ 5 Fg^{-1} at the 2000^{th} cycle with ~ 99% retention.

5. NOVEL FABRICATION OF $NiWO_4$ DECORATED, LIGNIN BASED NOVEL ELECTRODES

In the earlier chapter we studied the capacitive performance and drawbacks of the electrode made from the lignin, decorated with a transitional metal oxide (MnO_2) particles. In this chapter, in order to overcome the drawbacks, efforts have been made to develop new materials. The nanoparticles were fabricated cost-effectively, and can easily be manufactured in large quantity. Decoration of $NiWO_4$ ions on this lignin matrix was done to increase the electroactive surface area, and in turn, increase the electrochemical conductivity of the material. The interaction of lignin and these new nanoparticles have been analyzed using three electrochemical tests; Cyclic Voltammetry (CV), Cyclic Charge-Discharge (CCD) and Electrochemical Impedance Spectroscopy (EIS).

5.1. Synthesis of Nickel Tungstate nanomaterials ($NiWO_4$)

Nickel tungstate nanoparticles have been prepared by a simple wet chemical route at room temperature (Figure 5.1). For this synthetic route, 0.5 M of nickel acetate tetra hydrate was mixed with 100 ml of distilled water until to get a homogeneous solution under magnetic stirred condition. Similarly, 0.2 M of sodium tungstate was mixed with a required amount of distilled water. Homogeneous solution of sodium tungstate was added by drop wise manner in to an aforementioned nickel acetate solution. A greenish blue precipitate was observed. The mixture was maintained under stirred condition for 1hr and the obtained precipitate was centrifuged and dried.

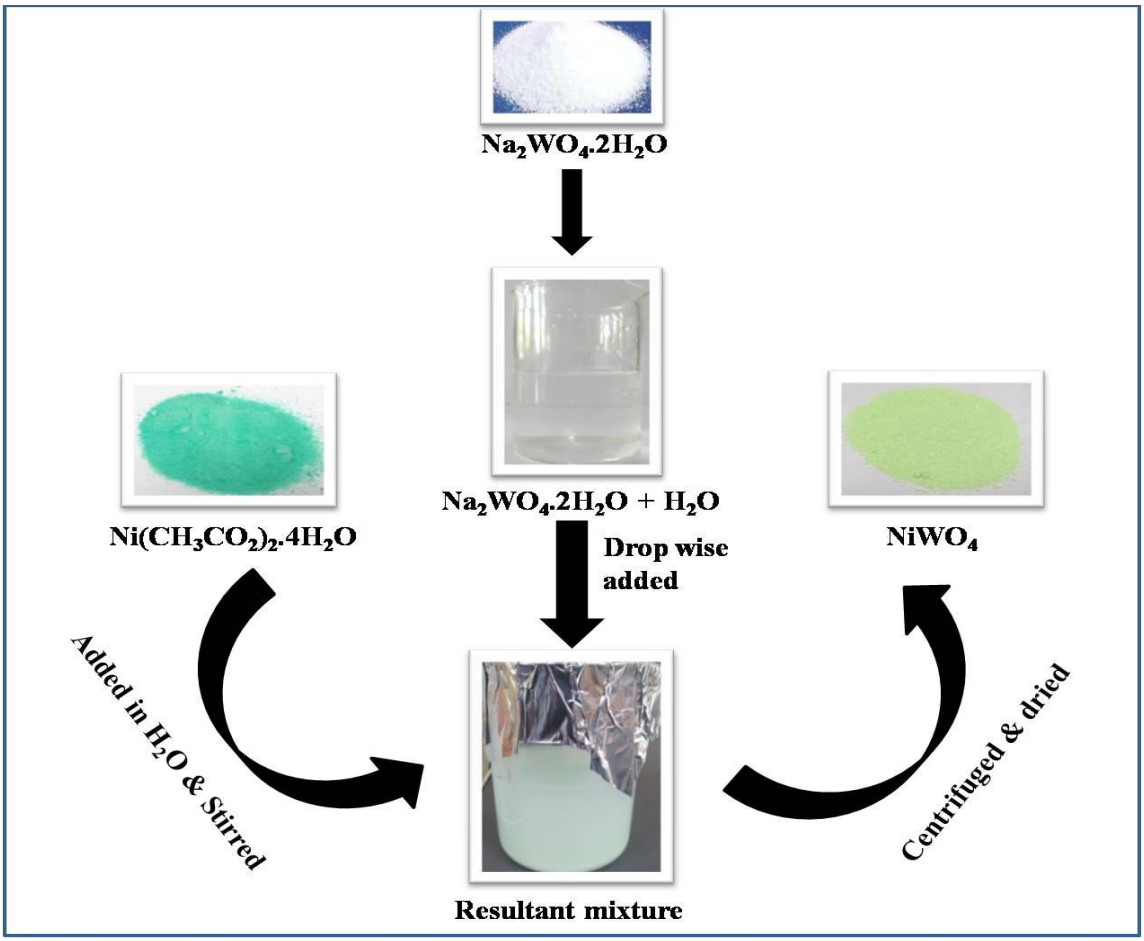

Figure 5.1: Schematic representation of $NiWO_4$ synthetic procedure

5.2. Preparation of lignin-$NiWO_4$ Composite Electrode

First, the $NiWO_4$ nanoparticles were added to lignin and mixed with PVDF in 3 different molecular weight ratios of Lignin: $NiWO_4$: PVDF. The 3 ratios chosen were 80:10:10 (L-80), 45:45:10 (L-45), and 10:80:10 (L-10). 2 ml of NMP was added to the powder to form the slurry. The slurry was coated on an aluminum foil (0.98 mm thick) substrate cut in the form of a circular plate of diameter 4 cm. The adjoining strips of the foil were 1 cm wide

and 3 cm long. The coated foil was heated in a vacuum oven for 4 hours at 100°C to obtain the lignin-$NiWO_4$ composite electrode.

5.3. Preparation of PVA/H_3PO_4 Gel Electrolyte

The method for the preparation of the electrolyte has been explained in chapter 3, section 3.2. No details will be repeated here.

5.4. Assembly of Solid-state Asymmetric Supercapacitor

The asymmetric supercapacitor is made up of $NiWO_4$ decorated lignin (lig) as the active material. With Al/ lig-$NiWO_4$ as the anode and Al/AC as the cathode. The assembly of this solid-state supercapacitor is shown in Figure 5.2.

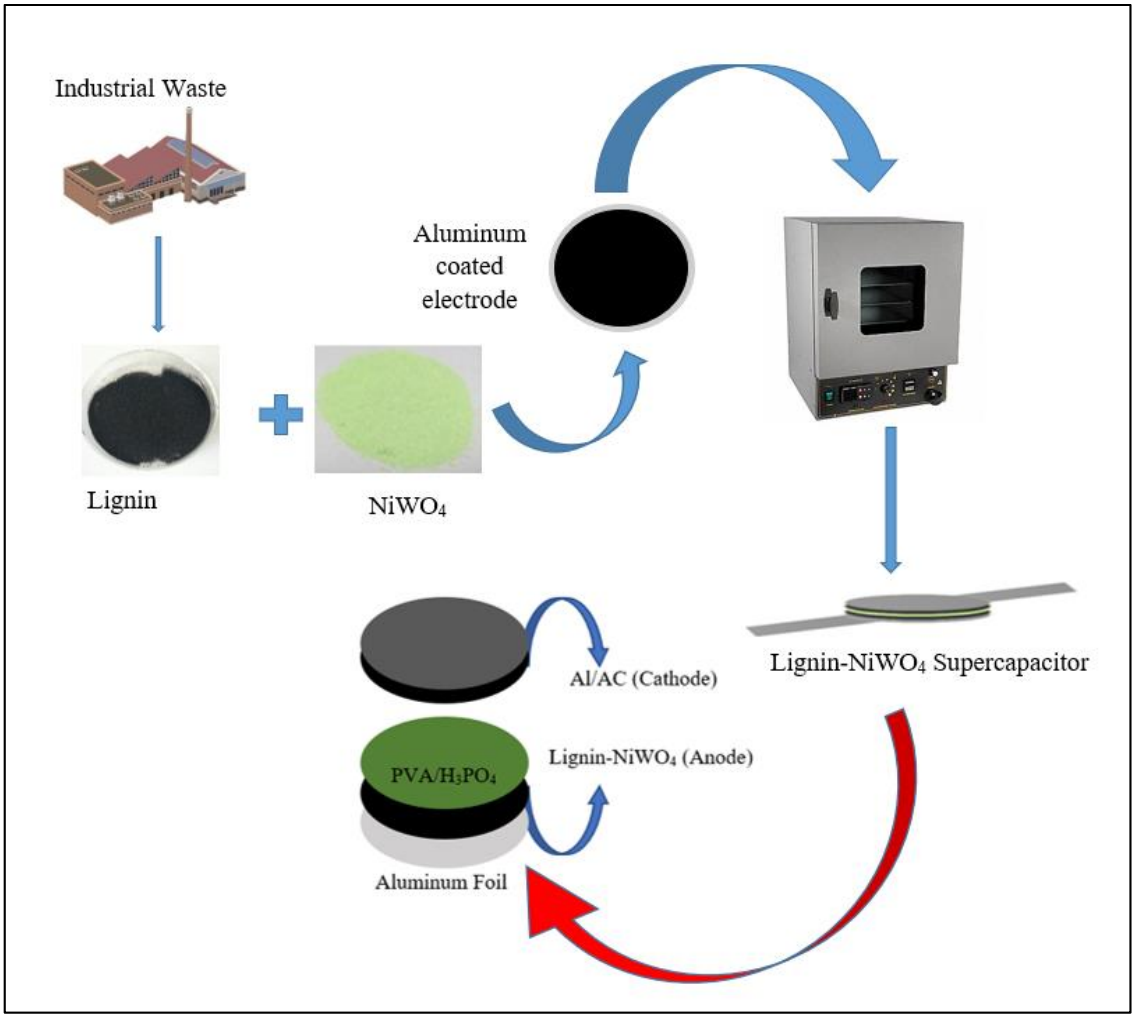

Figure 5.2: Schematic Process of Solid-state Asymmetric Supercapacitor

5.5. Morphology Characteristics

In morphological aspects, scanning electron microscopy (SEM) images has been taken and the corresponding images were given as Figure 5.3 (a-b). Figure 5.3 (a-b) are the higher and lower magnification images of $NiWO_4$. From these images, uniform distribution of the material and size of the material can clearly visualized. This uniform distribution attributes to the high contact area.

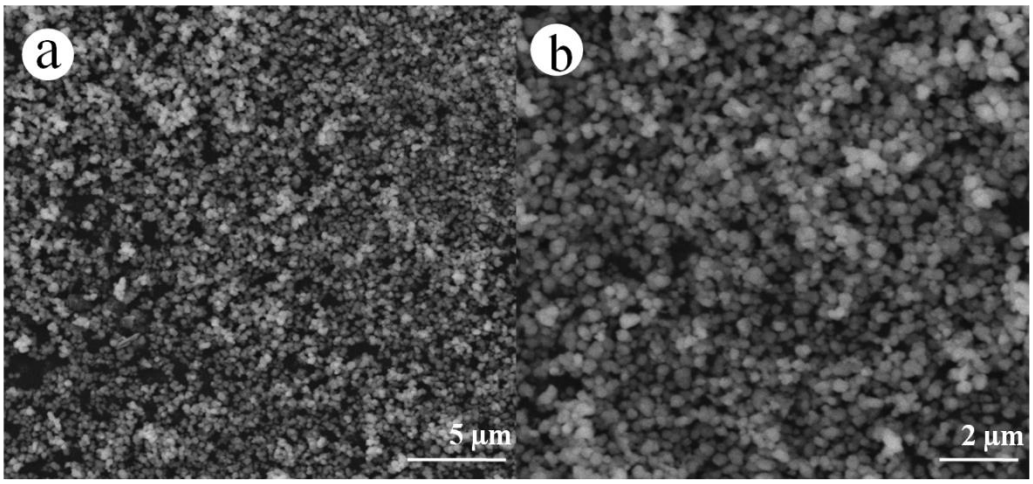

Figure 5.3 (a-b): High and low magnification SEM analysis of $NiWO_4$ nanomaterials

5.6. Electrochemical Capacitive Performance

The electrochemical performance of the 3 different samples is tested using cyclic voltammetry (CV), cyclic charge-discharge (CCD) experiments and electrochemical impedance spectroscopy. The samples were named in the order lig:$NiWO_4$:PVDF, the numbers indicate the weight percentage for each component. For instance, 10:80:10 symbolizes 10 % lignin, 80 % $NiWO_4$ and 10 % PVDF by weight. The 3 samples, their ratios and their names are mentioned in Table 1.

Table 1: Sample Names & Ratios

S.No.	Sample Name	Weight % (Lig:$NiWO_4$:PVDF)
1)	L-80	(80:10:10)
2)	L-45	(45:45:10)
3)	L-10	(10:80:10)

5.6.1. Cyclic Voltammetry (CV) Test

The voltage range for the CV test for all 3 samples was selected as 1-2 volts. This voltage range was selected based on lignin's performance for different voltage ranges in the previous experiments. The CV test was run for 4 scan rates (100, 50, 25, & 10 mVs^{-1}). For comparison purposes, the CV curves obtained at the scan rate 10 mVs^{-1} are shown in Figure 5.4(a). This scan rate was selected for comparison because at scan rates higher than 10 mVs^{-1}, the scan voltage rate is too fast while for scan rate lower than 10 mVs^{-1}, it is too slow for a stable system dynamic. In Figure 5.4(a), it can be seen that as the amount of lignin decreases the specific capacitance of the system increases. The highest value of specific capacitance obtained is 15.1 Fg^{-1} (2.4 mFcm^{-2}) for sample L – 10. The lowest value of specific capacitance obtained is 0.5 Fg^{-1} (8.4 mF cm^{-2}) which is the least.

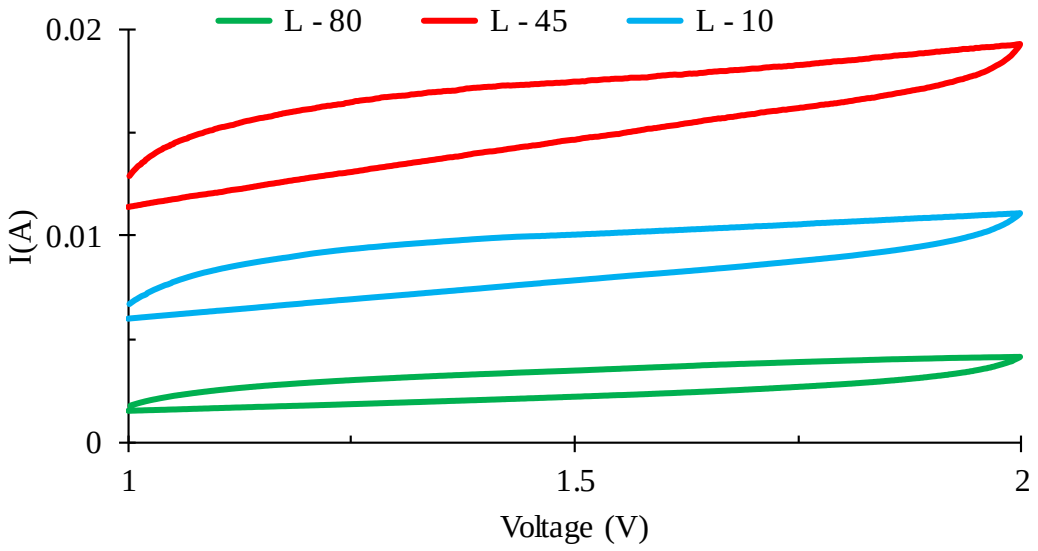

(a)

Figure 5.4: (a) CV curves obtained for the 3 samples for voltage range 1-2 V at 10 mVs^{-1}. (b) Variation of specific capacitance for the 3 samples

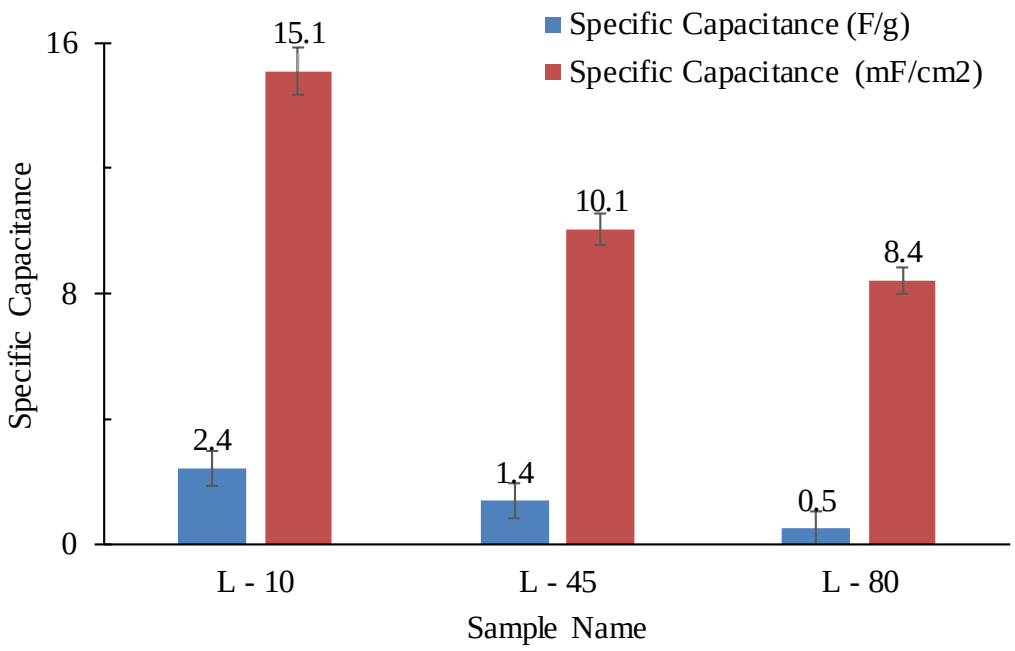

(b)

Figure 5.4 Continued

5.6.2. Cyclic Charge-Discharge (CCD) Test

To assess the capacitance performance of the 3 samples, CCD experiment was carried out at the same current density of 0.13 Ag^{-1} for 600 cycles each. The variation of areal specific capacitance with cycles is shown in Figure 5.5(a) for first 600 cycles. Areal specific capacitance retention is shown in Figure 5.5(b). It is seen from Figure 5.5(a) that the areal specific capacitance for the sample L - 10 is the highest throughout (~17.01 mF cm^{-2}) followed by the samples L - 45, and L – 80. This confirms the behavior observed in the CV experiment that as lignin content increase, the specific capacitance decreases. The order of the final retention, however, follows the order L – 10 > L – 80 > L – 45 (Figure 5.5(b)).

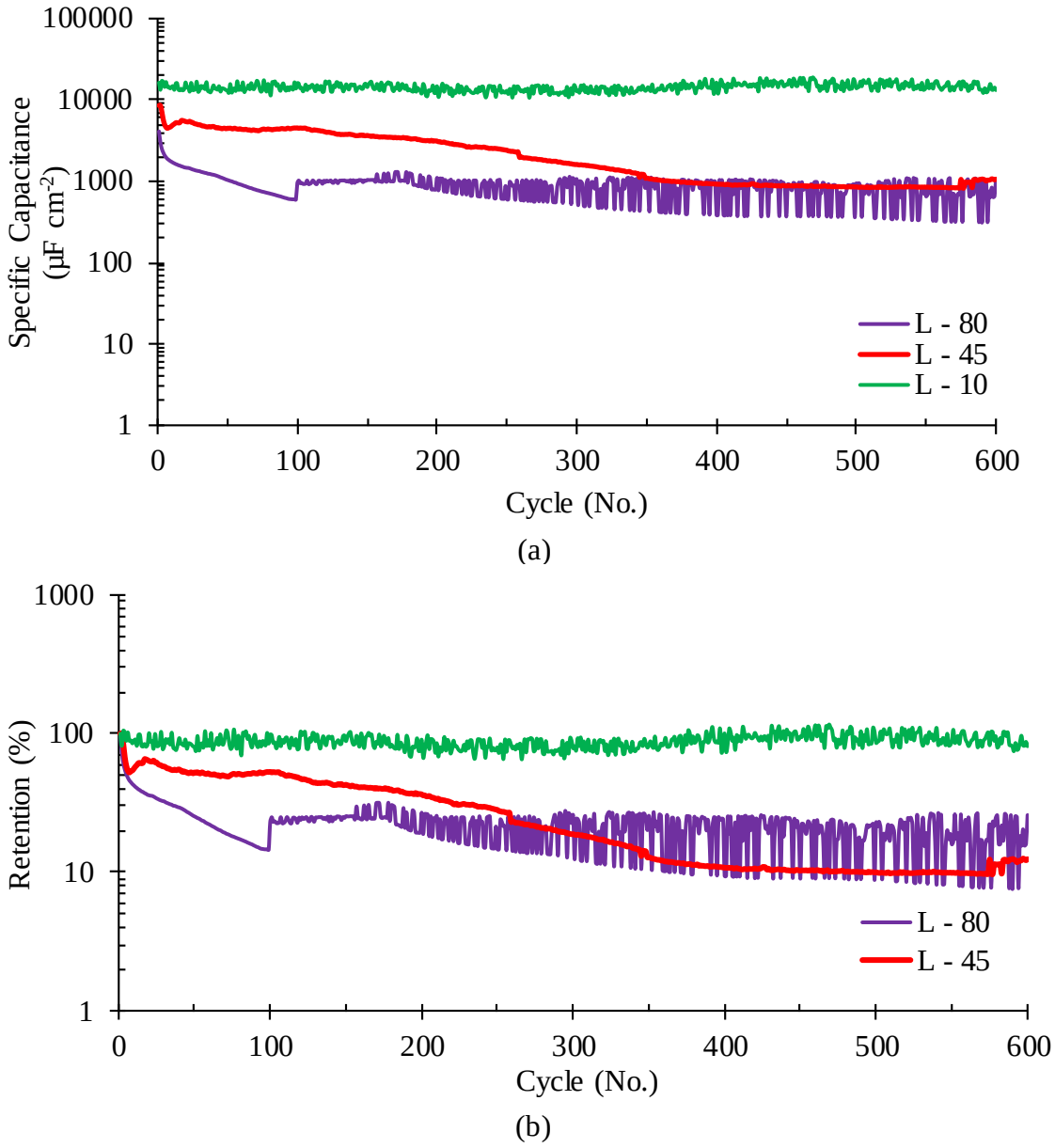

Figure 5.5: (a) Variation of specific capacitance with cycles for CCD experiment for 3 samples at a current density of 0.13 Ag^{-1} for 600 cycles each. (b) Capacitance retention (%) vs. Cycle (No.) plot for CCD experiment for 3 samples

As per the results, CCD experiment was carried out for the best sample L - 10 at a current density of 0.13 Ag^{-1} for 2000 cycles. The variation of specific capacitance with cycles for

the cyclic charge-discharge experiment for Sample L - 10 is shown in Figure 5.6(a). The y-axis is shown in log scale. The experiment is run for 2000 cycles. The specific capacitance seems to be stable as the number of cycles increase. The maximum value of the specific capacitance is ~ 5.28 Fg^{-1} (32.9 mF cm^{-2}) at the first cycle while the minimum value is ~ 3.52 Fg^{-1} (21.92 mF cm^{-2}) at the 2000th cycle. There is a very small and slow decline in the value of the specific capacitance.

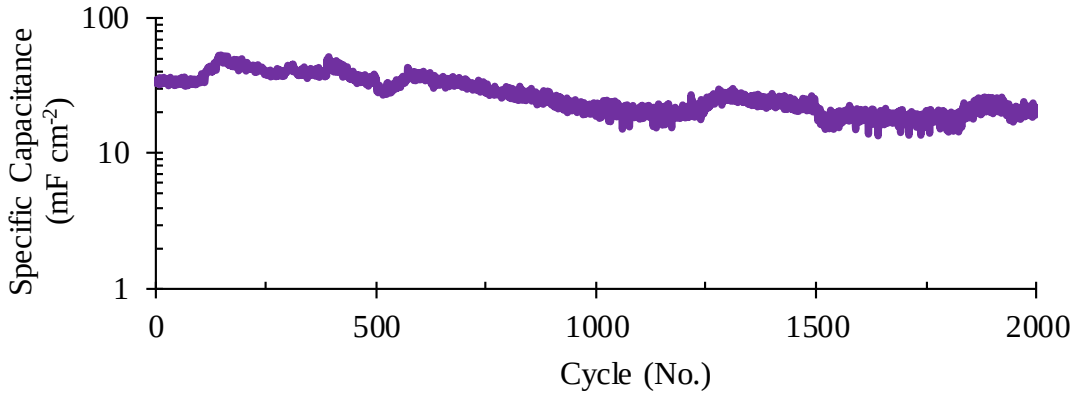

(a)

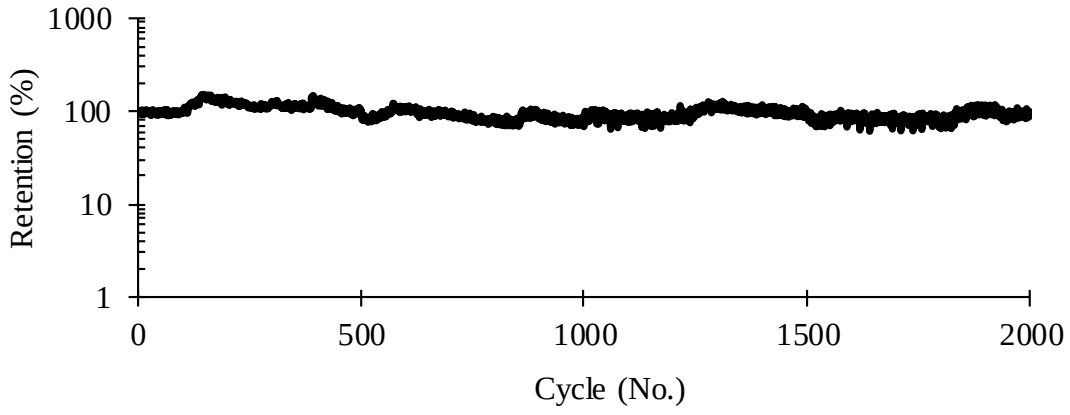

(b)

Figure 5.6: (a) Variation of specific capacitance with cycles for CCD experiment of sample L – 10 at current density of 0.13 Ag^{-1} for 2000 cycles. (b) Capacitance retention (%) vs. Cycle (No.) plot for CCD experiment of sample L – 10

For the CCD experiment, the capacitance retention for the supercapacitor is calculated and the retention % is plotted for 2000 cycles accordingly in Figure 5.6(b). The capacitance retention declines from an initial value of 100 % to ~ 85 % after 2000 cycles. The trend of retention is non-monotonic. For every 1000 cycles interval, the first interval shows a very slow decline, the second interval shows consistency. Thus, a threshold value of specific capacitance, and corresponding energy and power densities, can be easily determined (using the value at the start of the last interval, i.e. at the 1000th cycle) at which the supercapacitor can be used with ~ 98 % retention for the entire 2000 cycles for many electronic devices which operate within that specific capacitance range. This retention behavior may work well with devices that require variable power or energy after some usage.

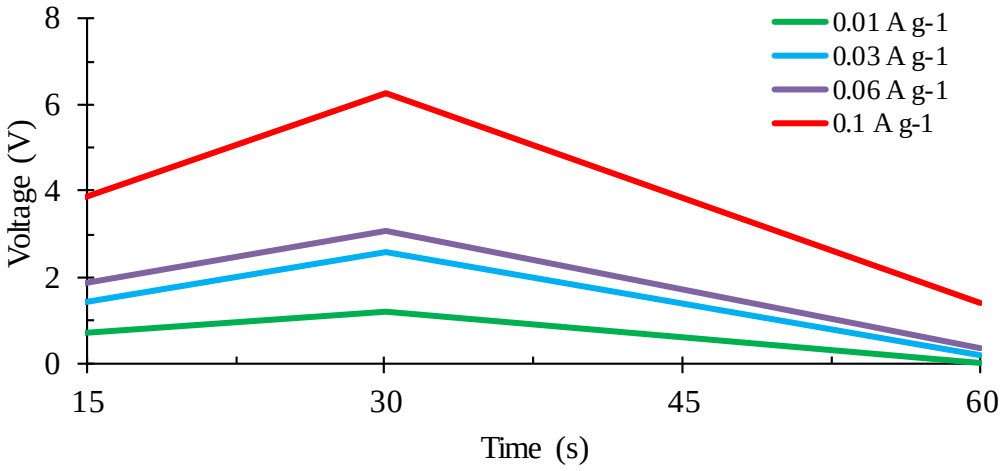

(a)

Figure 5.7: Comparative plots of (a) voltage versus time at different current densities, (b) specific capacitance versus current density in the cyclic charge discharge experiment, (c) Plots of energy density (black) and power density (red) versus cycles, and (d) Ragone plot of the lig- $NiWO_4$ supercapacitor.

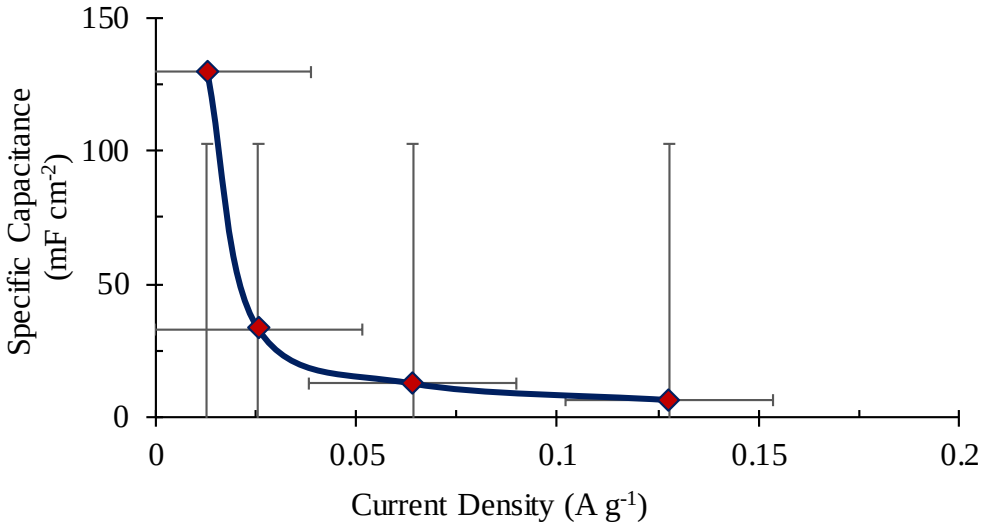

(b)

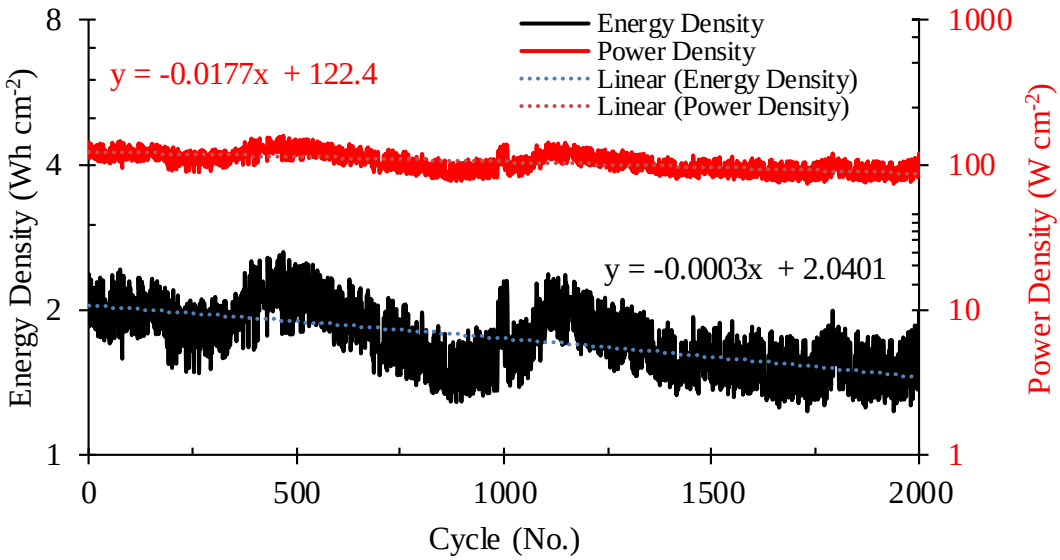

(c)

Figure 5.7 Continued

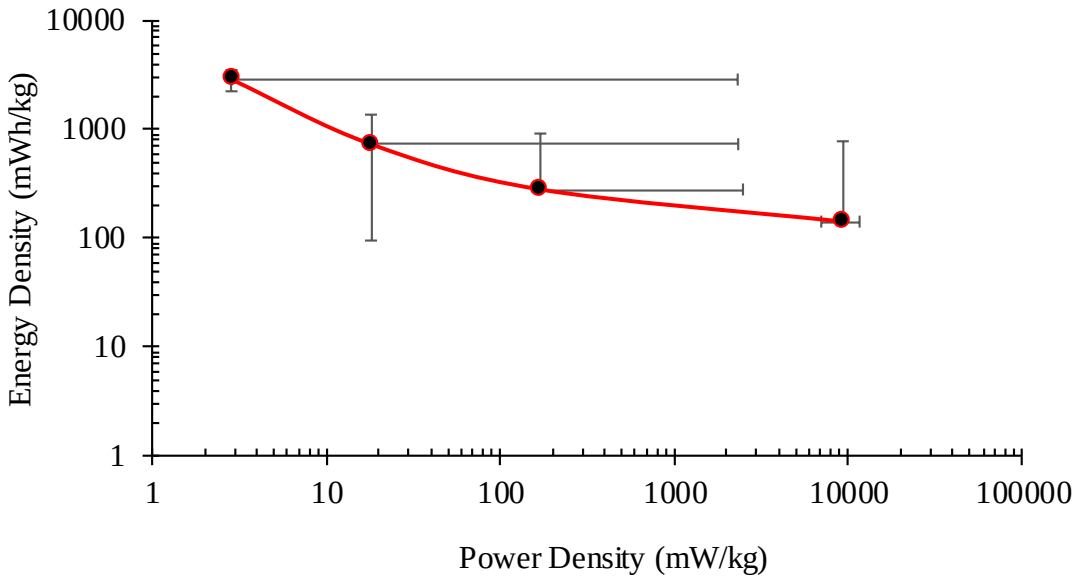

(d)

Figure 5.7 Continued

To observe the impact of current density on the resultant discharge voltage in the cyclic charge-discharge experiment, Figure 5.7(a) is obtained. The resultant voltage curves are obtained at various current densities of 0.01 A/g (green), 0.03 A/g (sky blue), 0.06 A/g (orange), and 0.1 A/g (red). The rate of decline (slope) of the discharge voltage curves varies with varying current densities. The higher the current density is, steeper is the slope of the voltage-time curve. Thus, at higher current density the voltage drop is at a higher rate. This is an expected behavior for any supercapacitor.

To obtain the effect of discharge current density on specific capacitance, Figure 5.7(b) is obtained for a constant charge current of 2 mA. The specific capacitance declines with increasing discharge current density. This too is reflective of the behavior of any supercapacitor. Figure 5.7(c) shows the variation of energy density (black) and power

density (red) with cycles. A linear fit (equation shown on the plot) with a very small negative slope (0.0003) indicates negligible decay in the energy density value. The intercept for this fit is 2.04. Thus, it is observed that the energy density varies about a mean value of 2 Wh cm^{-2}. Similarly, when a linear fit is used for the power density plot, we observe a very small negative slope (-0.017) indicative of very slow decay. The intercept for this fit is 122.4 Thus, it is observed that the power density varies about a mean value of 100 W cm^{-2}. A Ragone plot (Figure 5.7(d)) is shown for the supercapacitor which shows the variation of the energy density with the power density at varying current densities as obtained from the cyclic charge-discharge experiment. The nature of the curve is consistent with those reported for metal oxide-based supercapacitors. Here we have a concave upwards decline instead of the usual convex upwards decline for the energy density.

5.6.3. Electrochemical Impedance Spectroscopy (EIS)

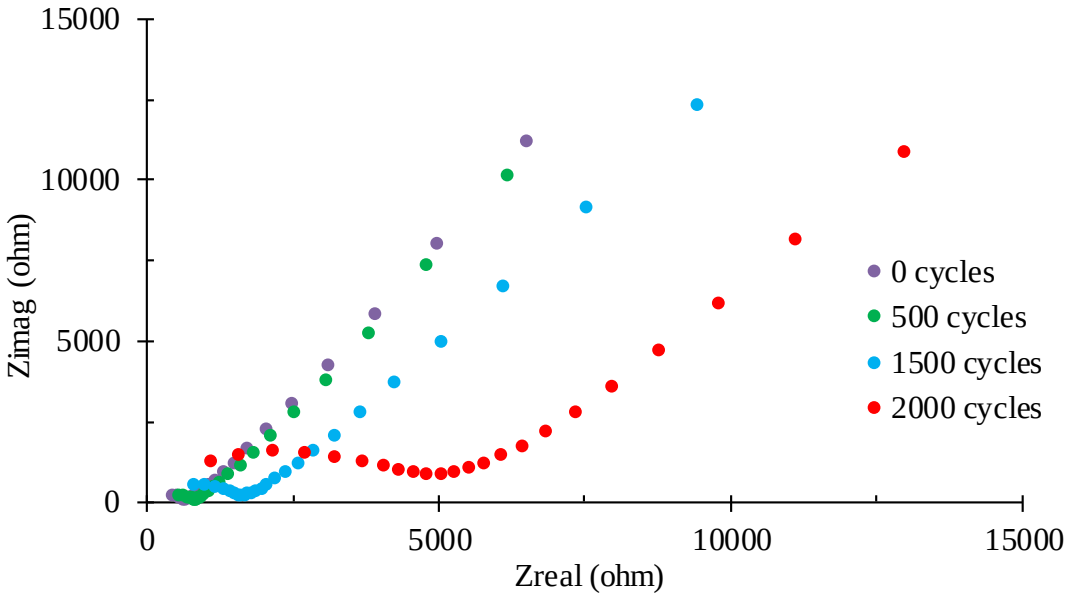

Figure 5.8: Electrochemical impedance spectroscopy (Nyquist plots)

Electrochemical impedance spectroscopy was carried out to understand the impedance behavior of the supercapacitor, and accordingly, the Nyquist plots are obtained and shown in Figure 5.8. For the sample L – 10, the total impedance at the beginning (yellow) is about 500 ohm which is smaller than 1000 ohm, the value after the 500th cycle (green). Similarly, the impedance after the 1500th cycle (blue) is 1620 ohm which is smaller than that after the 2000th cycle (red). The impedance values follow the trend 0th, 500th, 1000th, 1500thand 2000th cycle from the least to the greatest. This indicates that with the progression of cycles, the resistance to current flow increases, and hence it results in lesser current flow and lesser capacity retention towards higher cycle number. The rate at which impedance develops, however, is steeped towards the end, i.e. from the 1500th to the 2000th cycle.

5.7. Summary

Solid-state asymmetric supercapacitors were assembled, with $NiWO_4$ decorated lignin (lig) as the active material, Al/ lig-$NiWO_4$ as the anode and Al/AC as the cathode. The electrolyte used was PVA/H_3PO_4 gel polymer. 3 samples of different weight % ratios were made and tested. Using the CV and CCD test, it was proved that as lignin content increases, specific capacitance decreases. Sample L – 10 showed the highest specific capacitance and retention. It was run further for 2000 cycles. The system showed very good stability and retention. The highest specific capacitance obtained was ~ 5.28 Fg^{-1} at the first cycle while the minimum value is ~ 3.52 Fg^{-1} at the 2000^{th} cycle with ~ 98% retention.

6. CONCLUSIONS AND FUTURE RECOMMENDATIONS

6.1. Conclusions

This research investigated novel electrodes that are lightweight, low cost, and plant-based, flexible as supercapacitors. The electrodes are designed and constructed using Al substrate, with an organic gel polymer electrolyte, PVA/H_3PO_4. The use of a gel electrolyte eliminates the risk of leakage of the electrolyte. Since the electrolyte is organic, that makes environmentally friendly. The main objective was of this research was to build an eco-friendly, low-cost, light-weight, and flexible solid-state supercapacitor electrodes made from plant-based materials. For this purpose, the biomaterial lignin was selected to be studied, tested and analyzed. Three different studies were conducted to study the lignin interactions with another biomaterial, with a transition metal oxide (MnO_2), and with newly synthesized nanoparticles ($NiWO_4$).

Utilization of lignin as an active material for the anode in combination AC as the cathode has shown various advantages, like:

- Stability of the interface - the smoother AC particle surface, observed by the negative kurtosis value for AC against positive value for lignin, helps in strong attachment of the cathode layer with the electrolyte layer resulting in better contact for electrochemical reactions.
- High contact area - the high porosity of AC particles, as well as the pore distribution in $NiWO_4$ nanoparticles, observed in the SEM image, gives an added advantage of enhanced surface area of contact.

- Strong adhesion - The even distribution of AC particles, observed from SEM images, contributes to better attachment due to adhesion.

For the AC/Lig-MnO_2 supercapacitor, by adding lignin to active carbon, the packing density of the electrode is significantly improved. This results in a high surface area for electrochemical reactions. Lignin particles have a more elongated shape than that of AC particles. The electrode surface has micron-sized AC particles distributed evenly, and the gel surface is smooth. The AC electrode surface is porous, and the AC particles are seen evenly distributed throughout the electrode surface resulting in better attachment and higher contact area with the electrolyte. In addition, using lignin and AC combination has a distinct advantage of the higher surface packing density of lignin and low surface roughness of AC. The attachment of the layers and uniformity of thickness can both be improved with more stringent process design and assembly.

For the Lig-$NiWO_4$ supercapacitor, due to the synergistic effect of activated carbon, lignin, and NiWO4, the fabricated AC/ lig-NiWO4 supercapacitor has superior performance than currently reported. Such electrochemical performance of this supercapacitor makes it useful for a wide variety of device applications which employ flexible supercapacitors. This work thus not only demonstrates distinct advantage of using lignin in combination with AC but also explores the surface morphology feature of the electrode surface.

Optimization of all constituents of the lignin-based supercapacitor is done to quantitatively justify the use of these constituents and to obtain consistent performance. It is not only complicated but also a challenging task to commercialize the use of bio-derived materials for electronics due to the instabilities exhibited in electrochemical capacitive performance. This work makes a practical attempt to obtain an enhanced and consistent electrochemical performance through cost effective measures. The two key and essential outcomes emphasized in this work are:

1) Combination of lignin in certain specific ratios with transitional metal oxide particles or/and with another biomaterial can have a tremendous effect on the capacitive performance and retention of supercapacitors.
2) Through optimization of constituent ratios of novel transition metal oxide nanoparticles in combination with lignin, it is possible to obtain electrochemical performance which is not only at par with many state-of-art devices but even better in many cases.

This work used a novel fabrication route of using plant-based raw material in solid-state flexible supercapacitors. Due to the simple and cost-effective method used, and raw materials derived from green sources, this work could mark an important step towards green technology development.

6.2. Future Recommendations

In this research, the electrochemical properties of unprocessed pure alkali lignin were studied. It showed tremendous potential to be used not only as a carbon precursor, but also as an active material for electrodes. When combined with another biomaterial or new nanoparticles, the performance improved further and the system showed very good stability and energy retention. To use lignin as an active material, further research is required. Studying and understanding the interactions of lignin with different materials is the first step. The use of different substrates, conducting polymers, other metal oxides and nanoparticles, and organic gel polymer electrolytes may improve the energy retention. The potential shown by lignin can lead to the development of eco-friendly, low-cost, and highly effective electrodes for batteries and supercapacitors.

REFERENCES

1. Youe WJ, Kim SJ, Lee SM, Chun SJ, Kang J, Kim YS. *MnO2-deposited lignin-based carbon nanofiber mats for application as electrodes in symmetric pseudocapacitors*. Int J Biol Macromol. 2018;112:943-950.

2. Lu W, Dai L. *Carbon nanotube supercapacitors.* Carbon Nanotubes: IntechOpen; 2010.

3. Pfaltzgraff LA, Cooper EC, Budarin V, Clark JHJGC. *Food waste biomass: a resource for high-value chemicals*. 2013;15(2):307-314.

4. Lota G, Tyczkowski J, Makowski P, Balcerzak J, Lota K, Acznik I, et al. *The modified activated carbon treated with a low-temperature iodine plasma used as electrode material for electrochemical capacitors*. 2016;175:96-100.

5. Faraji S, Ani FN. *The development supercapacitor from activated carbon by electroless plating—A review*. Renewable and Sustainable Energy Reviews. 2015;42:823-834.

6. González JF, Román S, Encinar JM, Martínez G. *Pyrolysis of various biomass residues and char utilization for the production of activated carbons*. Journal of Analytical and Applied Pyrolysis. 2009;85(1):134-141.

7. Yahya MA, Al-Qodah Z, Ngah CWZ. *Agricultural bio-waste materials as potential sustainable precursors used for activated carbon production: A review*. Renewable and Sustainable Energy Reviews. 2015;46:218-235.

8. Poletto M, Ornaghi HL, Zattera AJ. *Native Cellulose: Structure, Characterization and Thermal Properties*. 2014;7(9):6105-6119.

9. Béguin P, Aubert JP. *The biological degradation of cellulose*. FEMS Microbiology Reviews. 1994;13(1):25-58.

10. Li Y, Li W, Zhang G, Lü X, Hwang H, Aker WG, et al. *Purification and characterization of polysaccharides degradases produced by Alteromonas sp. A321*. Int J Biol Macromol. 2016;86:96-104.

11. Vanholme R, Demedts B, Morreel K, Ralph J, Boerjan W. *Lignin Biosynthesis and Structure*. Plant Physiology. 2010;153(3):895.

12. Sun Y, Cheng JJBt. *Hydrolysis of lignocellulosic materials for ethanol production: a review*. 2002;83(1):1-11.

13. Shafizadeh F, Bradbury AJJoaps. *Thermal degradation of cellulose in air and nitrogen at low temperatures*. 1979;23(5):1431-1442.

14. Sanchez OJ, Cardona CAJBt. *Trends in biotechnological production of fuel ethanol from different feedstocks*. 2008;99(13):5270-5295.

15. Mok WSL, Antal Jr MJJI, Research EC. *Uncatalyzed solvolysis of whole biomass hemicellulose by hot compressed liquid water*. 1992;31(4):1157-1161.

16. Chen Y, Sharma-Shivappa RR, Keshwani D, Chen CJAb, biotechnology. *Potential of agricultural residues and hay for bioethanol production*. 2007;142(3):276-290.

17. Chang VS, Holtzapple MT, editors. *Fundamental factors affecting biomass enzymatic reactivity*. Twenty-first symposium on biotechnology for fuels and chemicals; 2000: Springer.

18. Carvalheiro F, Duarte LC, Gírio FMJJoS, Research I. *Hemicellulose biorefineries: a review on biomass pretreatments*. 2008:849-864.

19. Kumar R, Wyman CEJBp. *Effects of cellulase and xylanase enzymes on the deconstruction of solids from pretreatment of poplar by leading technologies*. 2009;25(2):302-314.

20. Sun R, Lawther JM, Banks WJIc, products. *Influence of alkaline pre-treatments on the cell wall components of wheat straw*. 1995;4(2):127-145.

21. Taherzadeh M, Karimi KJIjoms. *Pretreatment of lignocellulosic wastes to improve ethanol and biogas production: a review*. 2008;9(9):1621-1651.

22. Chang VS, Nagwani M, Kim C-H, Holtzapple MTJAb, biotechnology. *Oxidative lime pretreatment of high-lignin biomass*. 2001;94(1):1-28.

23. Kim S, Holtzapple MTJBT. *Delignification kinetics of corn stover in lime pretreatment*. 2006;97(5):778-785.

24. García-Cubero MT, González-Benito G, Indacoechea I, Coca M, Bolado SJBt. *Effect of ozonolysis pretreatment on enzymatic digestibility of wheat and rye straw*. 2009;100(4):1608-1613.

25. Vidal PF, Molinier JJB. *Ozonolysis of lignin—improvement of in vitro digestibility of poplar sawdust*. 1988;16(1):1-17.

26. Zhao H, Jones CL, Baker GA, Xia S, Olubajo O, Person VNJJoB. *Regenerating cellulose from ionic liquids for an accelerated enzymatic hydrolysis*. 2009;139(1):47-54.

27. Ghose T, Pannir Selvam P, Ghosh PJB, bioengineering. *Catalytic solvent delignification of agricultural residues: organic catalysts*. 1983;25(11):2577-2590.

28. Sun F, Chen HJBt. *Organosolv pretreatment by crude glycerol from oleochemicals industry for enzymatic hydrolysis of wheat straw*. 2008;99(13):5474-5479.

29. Mosier N, Wyman C, Dale B, Elander R, Lee Y, Holtzapple M, et al. *Features of promising technologies for pretreatment of lignocellulosic biomass*. 2005;96(6):673-686.

30. Chandra RP, Bura R, Mabee W, Berlin dA, Pan X, Saddler J. *Substrate pretreatment: the key to effective enzymatic hydrolysis of lignocellulosics?* Biofuels: Springer; 2007. p. 67-93.

31. Singh J, Suhag M, Dhaka AJCp. *Augmented digestion of lignocellulose by steam explosion, acid and alkaline pretreatment methods: a review*. 2015;117:624-631.

32. Pan X, Xie D, Gilkes N, Gregg DJ, Saddler JN, editors. *Strategies to enhance the enzymatic hydrolysis of pretreated softwood with high residual lignin content*. Twenty-Sixth Symposium on Biotechnology for Fuels and Chemicals; 2005: Springer.

33. Quiévy N, Jacquet N, Sclavons M, Deroanne C, Paquot M, Devaux JJPD, et al. *Influence of homogenization and drying on the thermal stability of microfibrillated cellulose*. 2010;95(3):306-314.

34. Alfani F, Gallifuoco A, Saporosi A, Spera A, Cantarella MJJoIM, Biotechnology. *Comparison of SHF and SSF processes for the bioconversion of steam-exploded wheat straw*. 2000;25(4):184-192.

35. Oliva JM, Sáez F, Ballesteros I, González A, Negro MJ, Manzanares P, et al. *Effect of lignocellulosic degradation compounds from steam explosion pretreatment on ethanol fermentation by thermotolerant yeast Kluyveromyces marxianus*. Biotechnology for fuels and chemicals: Springer; 2003. p. 141-153.

36. Schmidt AS, Thomsen ABJBT. *Optimization of wet oxidation pretreatment of wheat straw*. 1998;64(2):139-151.

37. Yang B, Wyman CEJB, Bioproducts, economy BIfas. *Pretreatment: the key to unlocking low-cost cellulosic ethanol*. 2008;2(1):26-40.

38. Kim KH, Hong JJBt. *Supercritical CO2 pretreatment of lignocellulose enhances enzymatic cellulose hydrolysis*. 2001;77(2):139-144.

39. Schacht C, Zetzl C, Brunner GJTJoSF. *From plant materials to ethanol by means of supercritical fluid technology*. 2008;46(3):299-321.

40. Zheng Y, Lin HM, Tsao GTJBp. *Pretreatment for cellulose hydrolysis by carbon dioxide explosion*. 1998;14(6):890-896.

41. Demirbas A, Arin GJEs. *An overview of biomass pyrolysis*. 2002;24(5):471-482.

42. Shafizadeh FJJoa, pyrolysis a. *Introduction to pyrolysis of biomass*. 1982;3(4):283-305.

43. Bridgwater AV, Kuester JL. *Research in thermochemical biomass conversion*: Springer Science & Business Media; 2012.

44. Beaumont OJW, Science F. *Flash pyrolysis products from beech wood*. 2007;17(2):228-239.

45. Demirbas MFJES, Part A. *Hydrogen from various biomass species via pyrolysis and steam gasification processes*. 2006;28(3):245-252.

46. Balat M. *Mechanisms of Thermochemical Biomass Conversion Processes. Part 1: Reactions of Pyrolysis*. Energy Sources, Part A: Recovery, Utilization, and Environmental Effects. 2008;30(7):620-635.

47. Dubal DP, Chodankar NR, Kim D-H, Gomez-Romero P. *Towards flexible solid-state supercapacitors for smart and wearable electronics*. Chemical Society Reviews. 2018;47(6):2065-2129.